Remote Sensing of Environment 280 (2022) 113222

Contents lists available at ScienceDirect

Remote Sensing of Environment

journal homepage: www.elsevier.com/locate/rse

Trend, seasonality, and abrupt change detection method for land surface temperature time-series analysis: Evaluation and improvement

Jing Li [a,b,c], Zhao-Liang Li [c,*], Hua Wu [a,b], Nanshan You [a,b]

[a] State Key Laboratory of Resources and Environment Information System, Institute of Geographic Sciences and Natural Resources Research, Chinese Academy of Sciences, Beijing 100101, China
[b] University of Chinese Academy of Sciences, Beijing 100049, China
[c] Key Laboratory of Agricultural Remote Sensing, Ministry of Agriculture and Rural Affairs/Institute of Agricultural Resources and Regional Planning, Chinese Academy of Agricultural Sciences, Beijing 100081, China

ARTICLE INFO

Edited by Jing M. Chen

Keywords:
Change detection methods
Time-series analysis
Land surface temperature
Evaluation

ABSTRACT

Long-term land surface temperature (LST) variation is vital for the study of climate change and environmental monitoring. Change detection methods provide access to recovery trajectories of trend and seasonality and detect abrupt changes in LST time series, but a comprehensive evaluation of the published methods is lacking. In this study, simulated LST data with a temporal resolution of 8 days under different scenarios were used to evaluate the performance of three commonly used methods: Detecting Breakpoints and Estimating Segments in Trend (DBEST), Breaks for Additive Seasonal and Trend (BFAST), and Bayesian Estimator of Abrupt change, Seasonal change, and Trend (BEAST). The results obtained using the simulated data indicated that BEAST was the best method for decomposing LST time series into trend and seasonality (mean RMSEs were 0.28 K and 0.27 K, respectively) and for detecting abrupt changes in these two components (mean F1 scores were 0.83 and 0.95, respectively). BFAST was less robust to high-complexity data (F1: 0.56 and 0.52, RMSE: 1.34 K and 1.46 K). 0.91 K and 1.29 K). DBEST is recommended to capture component details because it yields the least generalized output (F1 for trend: 0.37, RMSE: 0.64 K and 1.37 K). Both BFAST and DBEST exhibited reduced accuracy when the time-series data has long-lasting continuous missing data. An application using the 20-year MODIS LST time series supports the results obtained using the simulated data. BEAST exhibited the highest detection accuracy for land cover change (13 correct detections among 15 true changes), followed by DBEST (9) and BFAST (7). All three methods were ineffective for detecting low-magnitude disturbances: wildfires, heatwaves, and cold spells due to their low intensity or short duration. To reduce the non-negligible commission error of BEAST, this study proposes an improved BEAST, which eliminates the false breakpoints in BEAST using a set of thresholds. Compared with BEAST, the user accuracy of the improved BEAST was significantly increased by 13.9% in the simulated data, resulting in an F1 increase of 0.04, and 15 false breakpoints were eliminated among 53 detected disturbances in the MODIS LST time series. This study outlines commonly used change detection methods and offers guidance for choosing the optimal method to detect changes in LST time series. Furthermore, suggestions on the determination of parameters and false breakpoints elimination in the improved BEAST enable it more practical.

1. Introduction

Knowledge of long-term variation in land surface temperature (LST) is essential for understanding current environmental conditions and predicting future changes (Quan et al., 2016; Watts and Laffan, 2014). Such knowledge is increasingly important in view of climate change, hydrological cycle, vegetation monitoring, urban climates, and environmental studies (Li et al., 2013). With the continuous accumulation of satellite observations, LST time series mainly derived from satellite imagery, such as TM/ETM+/TIRS, AVHRR, AATSR, MODIS, and SEVIRI, have demonstrated their value for elucidating long-term variation in LST (Fu and Weng, 2016; Ghent and Remedios, 2013; Khorchani et al., 2018; Romaguera et al., 2018; Zhang et al., 2015).

The variation in LST time series can be divided into three groups. 1)

* Corresponding author.
E-mail address: lizhaoliang@caas.cn (Z.-L. Li).

https://doi.org/10.1016/j.rse.2022.113222
Received 20 January 2022; Received in revised form 20 May 2022; Accepted 12 August 2022
Available online 23 August 2022

Trend, that is, long-term gradual variation, which responds to climate change, land management, or land degradation (Lucht et al., 2006; Verbesselt et al., 2010a); 2) Seasonality. The Earth's motion around the Sun and the tilt of the Earth's axis cause daily insolation variation over the seasons of the year (i.e., seasonal variation), and this rhythm produces an annual temperature cycle (ATC); 3) Abrupt changes, caused by natural or anthropogenic disturbances (Potter et al., 2003) (e.g., climate changes, short-term climate fluctuations, fires, extreme weather, insect attacks, deforestation, urbanization, and farming). Moreover, knowledge of the seasonal abrupt changes in LST (such as changes in the dates of the last spring freeze and the first fall freeze) is necessary for agricultural monitoring and planting schedules. Understanding the three types of information will help to probe LST patterns and their drivers.

Previous efforts in LST time-series analysis have mainly employed interannual LST data to characterize trends and abrupt changes on an annual scale (Xing et al., 2020; Zhao et al., 2020). Interannual LST data come primarily from the annual synthetic data (e.g., annual mean LST, annual maximum LST, and annual minimum LST) or parameters of the annual temperature cycle (ATC) model (i.e., annual mean LST, annual amplitude, and annual phase) (Fu and Weng, 2018; Huang et al., 2016; Stine et al., 2009; Weng and Fu, 2014). Two types of change detection methods based on interannual LST data have been proposed: non-parametric and parametric. Combinations of the Theil-Sen slope and non-parametric abrupt tests, such as the Mann-Kendall test (Kendall, 1975; Mann, 1945; Sen, 1968; Theil, 1992), Spearman's rho tests (Lettenmaier, 1976; Sadmani et al., 2012), Pettitt's test (Pettitt, 1979), the Mann-Whitney *U* test (Mann and Whitney, 1947), and the moving *t*-test, are used to obtain the slope of the trend and detect abrupt changes. These methods have been widely applied for trend analysis of climatic, hydrological, and water resource variables (Konapala et al., 2020; Schaefer and Domroes, 2009; Tabari et al., 2014; Zhao et al., 2020). However, non-parametric methods are susceptible to the effects of time-series length, and the detected breakpoints are prone to drift (Jaiswal et al., 2015). In contrast, parametric methods fit time-series data with a given functional form (Mudelsee, 2019). Linear functions have been widely used for describing trends because of their simplicity (Hurrell, 1995; Tuomenvirta et al., 2000); however, the proportion of pixels with significant linear changes in global annual scale time-series LST was only 15.33% in the study of Xing (2020), therefore, it is cannot support the global temperature change analysis. Piecewise linear models provide insights into discontinuities in the LST time series and can identify a more accurate trend with abrupt changes (Karl et al., 2000).

However, the interannual time series ignores the intra-year variability of LST and cannot provide the specific timings of abrupt changes (Zhu, 2017). Using intra-annual LST time series (e.g., 8-day, 16-day, and

Table 1
A summary of the function, advantages, disadvantages, and application fields of the primary change detection methods.

Methods			Function	Advantages	Disadvantages	Applications	References
Change detection with unknown component forms	STL		Trend and seasonality decomposition	1) Able to deal with missing values in regularly spaced data 2) No special assumption for each component	1) No abrupt changes are provided 2) Parameters settings need to take into account data characteristics	Decompose time series of vegetation index (VI), LST, CO_2, etc. into trend and seasonality.	Robert et al., 1990; Jamali et al., 2015; Verbesselt et al., 2010b; Quan et al., 2016
	DBEST		1) Trend and seasonality decomposition 2) Abrupt changes detection in trend	Characterize both abrupt and non-abrupt changes in the trend component	1) The accuracy will decrease in the presence of high-frequency variation 2) Many thresholds and parameters can lead to different performance 3) Cannot deal with missing data	Vegetation change detection based on VI time series	Jamali et al., 2015; Wang et al., 2017
Change detection with known component forms	using full-time series	BFAST	1) Trend and seasonality decomposition 2) Abrupt changes detection in trend and seasonality	Distinguish trend abrupt change and seasonal abrupt change	1) Sensitive to the specification of the parameters 2) Cannot deal with missing data 3) Computationally expensive	LCC, fire detection, or trend and seasonal decomposition using time series of VI, reflectance, and LST	Verbesselt et al., 2010a, 2010b; Muro et al., 2018; Fu and Weng, 2016
		BEAST		1) Distinguish trend abrupt change and seasonal abrupt change 2) Reduce the uncertainty of the single best model in traditional methods by combining many competing models 3) Able to deal with missing values 4) Offer a rich set of diagnostic statistics to assist interpretation	1) Sensitive to the specification of parameters 2) Computationally expensive	LCC, ice storm, and fire detection based on VI time series; Reconstruction of LST time series	Zhao et al., 2019 Li et al., 2022
	Near-real-time change detection	CCDC, BFAST monitor, COLD, EWMACD	Abrupt changes in time series	1) High efficiency and timeliness 2) Able to deal with missing values	1) Frequently disturbances in time series may degrade the accuracy 2) Less helpful for subtle changes except for the EWMACD 3) Computationally expensive when used in long term-series change detection	Forest monitoring, LCC, and fire detection in near-real-time using time series of VI and reflectance.	Zhu and Woodcock, 2014; Zhu et al., 2020; Brooks et al., 2013; Verbesselt et al., 2012

monthly data) can simultaneously capture trend, seasonality, and abrupt change. Many change detection methods with intra-annual time series were developed to characterize trend, seasonality, and abrupt changes in vegetation index and reflectance, allowing for vegetation dynamic and land cover change (LCC) monitoring (Zhao et al., 2019). Methods with intra-annual time series can be roughly grouped into two categories: change detection with unknown component forms and change detection with known component forms. Table 1 provided a concise overview of the function, advantages, disadvantages, and application fields of the primary change detection methods.

(1) Change detection with unknown component forms

This type of method first iteratively estimates two components: trend and seasonality, and then detects abrupt changes by segmenting the trend or seasonality. Robert et al. (1990) first developed a Seasonal-Trend iterative decomposition procedure based on Locally weighted regression (STL). Based on the trend decomposed by the STL, Jamali et al. (2015) developed a trend estimation and segmentation method called Detecting Breakpoints and Estimating Segments in Trend (DBEST).

(2) Change detection with known component forms

This type of method defines the trend using a piecewise linear model and approximates the seasonality using a harmonic model (Browning et al., 2017; Brooks et al., 2012). Two types of such methods have been developed: change detection using full-time series and near-real-time change detection. In the first category of methods, which includes Breaks For Additive Seasonal and Trend (BFAST) (Verbesselt et al., 2010b), Bayesian Estimator of Abrupt change, Seasonal change, and Trend (BEAST) (Zhao et al., 2019), change detection in a times series can be solved by approximating the global optimum based on the given equation using full-time series. Near-real-time change detection methods aim to detect abrupt changes in near-real-time. Several well-known methods, such as BFASTmonitor (Verbesselt et al., 2012), Continuous Change Detection and Classification (CCDC) (Zhu and Woodcock, 2014), COntinuous monitoring of Land Disturbance (COLD) (Zhu et al., 2020), and Exponentially Weighted Moving Average Change Detection (EWMACD) (Brooks et al., 2013), first fit the decomposition model based on stable historical time series, then identify abrupt changes by looking for deviation in new observations calculated using the fitted model. To continuously detect abrupt changes in the time series, a new model needs to be fitted to the next stable historical time series until another change is identified.

Given a plethora of change detection methods and a large number of parameters to be defined, the selection of an optimal method and the definition of the parameters have become new challenges. Several studies have evaluated and compared the accuracy of some of these methods to LCC detection based on simulated or real NDVI and reflectance time series (Awty-Carroll et al., 2019; Saxena et al., 2018; Zhao et al., 2019). It has been demonstrated that BFAST outperformed most near-real-time methods (i.e., BFAST monitor, CCDC, and EWMACD). However, the setting of the parameters (e.g., the number of breakpoints) in BFAST has a significant impact on the detection outcomes. EWMACD was designed for detecting lower-magnitude changes in seasonality. CCDC exhibits weak accuracy due to its underfit to the seasonal curve. Additionally, near-real-time change detection methods require a stable historical period (at least two years) to fit the model. The changes that occurred in the historical period can bias the model's predictions, and frequent breaks will be likely to be missed. The recently developed change detection methods, i.e., DBEST and BEAST, adopted different inference paradigms from BFAST, but their advantages and weakness have not been well documented. Moreover, existing comparisons are mainly concerned with the accuracy of detecting abrupt changes to provide a basis for the selection of LCC detection methods, but neglect component decomposition performance.

Encouraged by the effectiveness of these change detection methods for characterizing changes in vegetation indices and reflectance time series, several efforts have been made to apply these methods to LST time series. BFAST was used to capture LST trends in response to LCC on wetlands (Muro et al., 2018). The variants of BFAST were employed to decompose LST time series, which supports the research of urban heat islands and the impact of LCC on LST (Quan et al., 2016; Fu and Weng, 2016). BEAST was used to reconstruct gap-free LST time series by summing decomposed trend and seasonality (Li et al., 2022). However, it remains unclear the accuracy of abrupt changes detection and trend-seasonality decomposition, as well as the difference in the performance of these methods. Therefore, a comprehensive evaluation of the applicability of primary published methods on LST time series is urgently needed.

To address the two issues mentioned above, the present study aimed to compare the performance of the component decomposition and abrupt change detection of these change detection methods using simulated and MODIS LST time series on an intra-annual scale. Besides BFAST (the most advanced method previously defined), the recently developed DBEST and BEAST were also included in the comparison to identify the optimal method and define the optimal parameters for LST change detection. Thus, our findings are useful for selecting optimal methods for global temperature change analysis.

2. Brief review of previous methods

Change detection methods can separate trend and seasonality from time-series data. Abrupt changes occur in both two components, and can therefore be considered as part of a trend or seasonality (Verbesselt et al., 2010b). The general form of the change detection method is defined in Eq. (1) and illustrated in Fig. 1. Time-series data equal the sum of the trend, seasonality, and remainder (Zhao et al., 2019),

$$Y_t = T_t + S_t + e_t, t = 1, \ldots, n \quad (1)$$

where Y_t (t denotes time) is the remotely sensed time series, T_t is the trend, S_t is the seasonality, the remainder e_t is the stochastic variation in variables, and n is the number of observations in time series. Given the general form, DBEST, BFAST, and BEAST were developed. The following section reviews the principles and formulations of these three methods.

2.1. DBEST

DBEST obtained linear segments of the trend component via trend estimation and trend segmentation (Jamali et al., 2015). In trend estimation, major discontinuities of a time series are firstly identified by level-shift points, which are detected by using a set of thresholds, including the level-shift thresholds (θ_1 *and* θ_2) and the duration threshold (D) (Fig. 2). Specifically, Level-shift points are verified by the two criteria: 1) the absolute difference (ΔY_t) between one level-shift point and the next data point is greater than θ_1; and 2) the absolute difference ($\Delta \overline{Y}_D$) of the mean values calculated over the period D before ($\overline{Y}_D$_before) and after ($\overline{Y}_D$_after) the current data point is greater than θ_2. Then, STL decomposition is performed for each segment separated by the level-shift points to estimate the trend and seasonality (Robert et al., 1990).

In trend segmentation, the turning points (i.e., breakpoints) are first identified based on rank statistics and sorted according to the local change in the trend. Then, the breakpoints are specified by minimizing the Bayesian information criterion (BIC) for least-squares fitting (Schwarz, 1978). The number of output breakpoints is determined by the maximum number of breakpoints m or the change-magnitude threshold ε. An overview of the processes in DBEST is shown in Fig. 3.

DBEST requires five user-defined parameters. θ_1, θ_2,and D are used to determine the accuracy of the trend estimation, and m or ε is used to

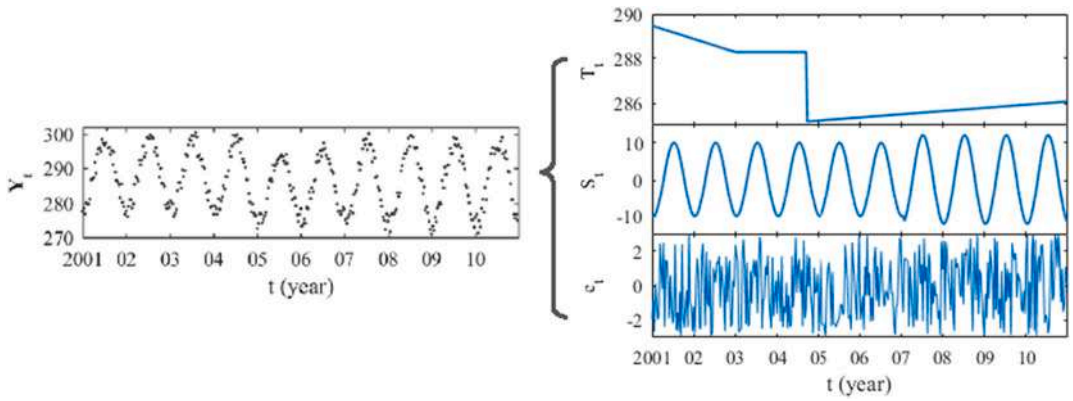

Fig. 1. Illustration of the general form of the change detection method: time-series observations (Y_t) equal the sum of the trend (T_t), seasonality (S_t), and remainder (e_t).

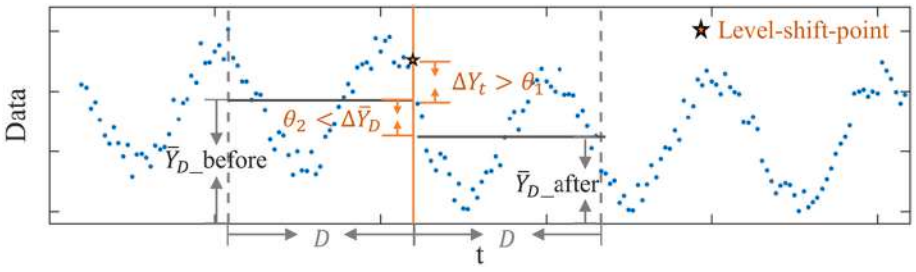

Fig. 2. Level-shift points (i.e., major discontinuities) detected by DBEST using the level-shift thresholds (θ_1*and* θ_2) and the duration threshold (D).

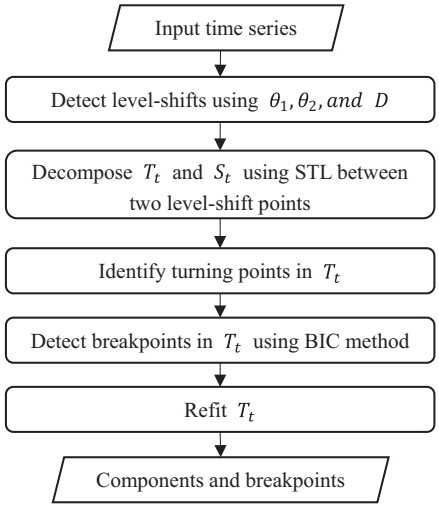

Fig. 3. Flowchart of DBEST for detecting trend abrupt changes in time series.

segment the trend and detect the breakpoints. DBEST outputs trend, seasonality, and the number, timing, and durations of trend abrupt changes. Although the principle of DBEST is simple, a large number of parameters must be determined. Moreover, DBEST is sensitive to high variation in de-seasonalized time series and is limited to regularly spaced data.

2.2. BFAST

BFAST employs an additive decomposition model to iteratively fit a trend and a seasonal model (Verbesselt et al., 2010b). It assumes that T_t is piecewise linear with $m + 1$ segments (i.e., m breakpoints: τ_1^*, …, τ_m^*):

$$T_t^i = \alpha_i + \beta_i \bullet t, \left(\tau_{i-1}^* < t \le \tau_i^*\right), i = 1, \ldots, m+1 \quad (2)$$

where T_t^i is the trend at segment i, α_i and β_i are the segment-specific slope and intercept, respectively. $\tau_0^* = 1$ and $\tau_{m+1}^* = n$. Similarly, the seasonality is fixed by $q + 1$ harmonic functions:

$$S_t^j = \sum_{h=1}^{H}\left[\gamma_{j,h} \bullet sin\left(\frac{2\pi ht}{P}\right) + \delta_{j,h} \bullet cos\left(\frac{2\pi ht}{P}\right)\right], \left(\tau_{j-1}^{\#} < t \le \tau_j^{\#}\right), j = 1, \ldots, q+1 \quad (3)$$

where S_t^j is the seasonality at segment j, q is the number of seasonal breakpoints ($\tau_1^{\#}$, …, $\tau_q^{\#}$), and $q + 1$ is the number of seasonal segments; $\tau_0^{\#} = 1$ and $\tau_{q+1}^{\#} = n$; P is the period of the seasonality and is a known parameter; H is the harmonic order, and $H = 3$ in BFAST; and $\gamma_{j,h}$ and $\delta_{j,h}$ are the segment-specific parameters for sine and cosine, respectively.

BFAST employed an iterative process to obtain the trend and seasonal components (Fig. 4). This process firstly initializes seasonality by using STL, followed by the detection of trend breakpoints, estimation of trend coefficients $\{\alpha_i, \beta_i\}$, detection of seasonal breakpoints, and estimation of seasonal coefficients $\{\gamma_{j,h}, \delta_{j,h}\}$. The process ends when the number and position of breakpoints are unchanged. The Ordinary Least Squares (OLS) residuals-based MOving SUM (MOSUM) test and least squares are used to determine the number and position of the breakpoints, and the component coefficients are estimated using a robust regression based on M-estimation.

When performing BFAST, three parameters must be defined: 1) the number of breakpoints, which refers to the maximum number of breakpoints in both trend (m) and seasonality (q); 2) the minimum separation size, which is calculated from the ratio of the minimum separation interval (ϕ) to the total length of the time series, and 3) the maximum number of iterations. The number of breakpoints is the most influential parameter in BFAST (Saxena et al., 2018). BFAST outputs trend and seasonality, and the number, timing, and confidence interval of abrupt changes in the two components. Although it is widely applied

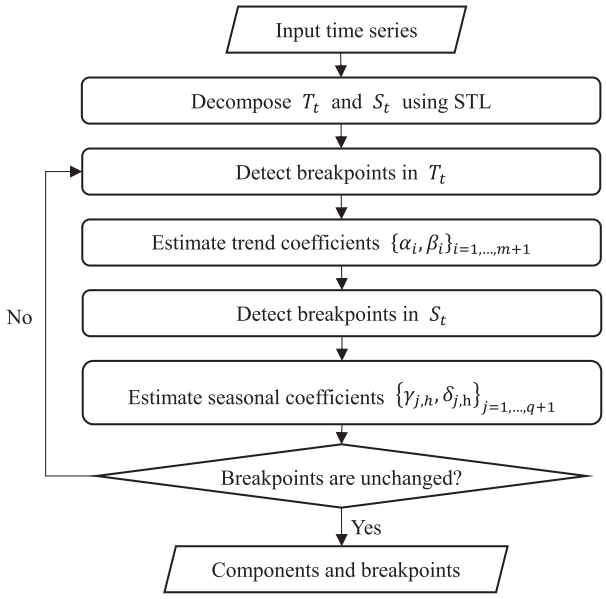

Fig. 4. Flowchart of BFAST for detecting abrupt changes in time series.

to detect changes in land surface conditions based on the vegetation index (VI), the performance of BFAST depends heavily on the parameters used (e.g., the minimum separation interval, number of breakpoints, and maximum number of iterations). Given that the OLS-MOSUM test for examining breakpoints requires regularly spaced data, BFAST cannot handle equally spaced time series with missing values.

2.3. BEAST

DBEST and BFAST employ the single-best-model paradigm that relies on locally-based heuristic rules and decompose the time series piece by piece and step by step. This paradigm is prone to model misspecification due to the single criteria and a large number of user-defined parameters. In contrast, BEAST synthesizes numerous competing models by assigning a probability based on the Bayesian Model Averaging (BMA) scheme (Denison et al., 2002). BEAST infers the number and positions of the breakpoints, and the coefficients in trend and seasonality in one step (Zhao et al., 2019).

BEAST also adopts a piecewise linear model and a piecewise harmonic model to parameterize the trend and seasonality based on Eqs. (2) and (3), respectively. However, BEAST does not require the specification of the harmonic order. The related parameters can be reclassified into two groups: model structure parameters M (i.e., number and timing of breakpoints in trend and seasonality, and harmonic order) and segment-specific coefficient parameters φ:

$$M = \{m\} \cup \left\{\tau_i^*\right\}_{i=1,\ldots,m} \cup \{q\} \cup \left\{\tau_j^{\#}\right\}_{j=1,\ldots,q} \cup \{H\} \tag{4}$$

$$\varphi = \{\alpha_i, \beta_i\}_{i=1,\ldots,m} \cup \left\{\gamma_{j,h}, \delta_{j,h}\right\}_{j=1,\ldots,q, h=1,\ldots H} \tag{5}$$

BEAST resorts to a Bayesian model to obtain the best values of these parameters, and their posterior probability distributions $p(\varphi, e_t, M|\{Y_t\}_{t=1,\ \ldots,\ n})$ are simulated by reversible-jump Markov Chain Monte Carlo (MCMC) sampling. Two types of parameters need to be determined: 1) model structure parameters, including the maximum number of breakpoints (m and q) and maximum harmonic order (H), and 2) simulation control parameters (e.g., sample number) for configuring the MCMC sampler in the Bayesian model. BEAST outputs trend and seasonality, the number, timing, occurrence probability, confidence interval of abrupt changes in the two components, and time-series seasonal harmonic orders. The probability of the breakpoints represents the severity of the disturbance in time series with a high signal-to-noise ratio. It is worth mentioning that, the processing of massive high-resolution data incurs daunting computation costs.

Based on the above description, Table 2 provides a comparison of the detection mechanism, input parameters, and output components of the three methods.

3. Data description

3.1. Simulated LST time series

We simulated the LST time series with a length of 10 years and a yearly period of 46, that is, with a temporal resolution of 8 days. The simulated time series (Y_t) was the sum of the simulated components of trend (T_t), seasonality (S_t), and remainder (e_t). These components had the following characteristics: a) Trend was simulated by a linear function. The slope of the trend ranged from −0.14 to 0.14 K per decade, considering that the LST has shown a long-term rise of 0.12 [0.08 to 0.14] K per decade over the period from 1951 to 2012 (IPCC. Stocker, 2014). The intercept (i.e., the initial LST) was set as 288 K; b) Seasonality was simulated by a harmonic function. The harmonic order was 1st or 2nd, the amplitudes changed from 20 to 40 K, and the phases varied from 1/9 to 1/3 period; c) Remainder, i.e., noise, was a series of random numbers ranging from −3 to 3 K, with a mean value of 0 K. Meanwhile, we simulated data missing scenario by randomly removing data points with certain proportions (0–40%). These scenarios imitate data discontinuities caused by clouds, snow, or the LST retrieval algorithm. The simulated trend, seasonality, remainder, and data missing were integrated to generate the basic time series. Then six datasets were simulated by using the basic time series. Fig. 5 displayed six examples randomly selected from these datasets (one example for each dataset). The characteristic of each dataset was explained as follows:

(1) Dataset 1: a total of 648 basic time series was directly employed to evaluate the performance of component decomposition.
(2) Dataset 2: one abrupt change was set in the trend component of the basic time series to evaluate the performance of abrupt change detection in trend. The abrupt change in different time series had different timing coordinates, different change

Table 2
Comparison of DBEST, BFAST, and BEAST used in this study.

Methods	Mechanism	Input	Output
DBEST	$Y_t = T_t + S_t + e_t$ Decomposes T_t and S_t using separated STL. Detects abrupt changes in T_t based on trend segmentation	Level-shift-threshold (θ_1*and* θ_2) and duration threshold (D); Maximum numbers of breakpoints in trend (m) or change-magnitude threshold (ε)	T_t and S_t; Abrupt changes and their duration in T_t
BFAST	$Y_t = T_t + S_t + e_t$ T_t: piecewise linear model S_t: piecewise harmonic model (harmonic order = 3) Iteratively decomposes data into T_t and S_t and detects abrupt changes	Maximum numbers of breakpoints in T_t (m) and S_t (q); Minimum separation interval (ϕ); Number of iterations	T_t and S_t; Abrupt changes and their confidence intervals in T_t and S_t
BEAST	$Y_t = T_t + S_t + e_t$ T_t: piecewise linear model S_t: piecewise harmonic model Simultaneously infers abrupt changes and T_t and S_t based on BMA	Maximum numbers of breakpoints in T_t (m) and S_t (q); Maximum harmonic order (H); minimum separation interval (ϕ); Sample number	T_t and S_t; Abrupt changes, their probabilities, and confidence intervals in T_t and S_t

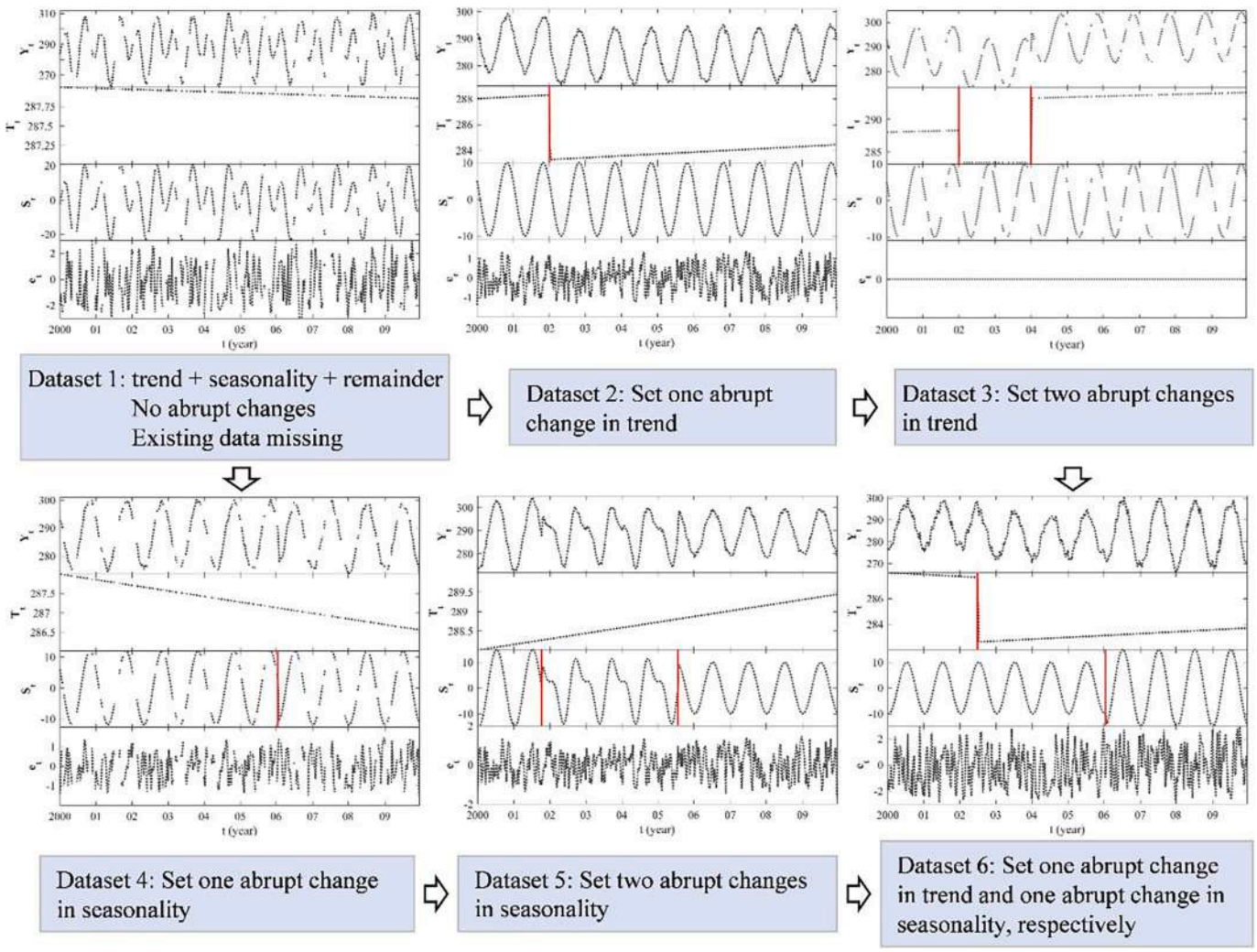

Fig. 5. Illustration of six typical simulated time series (one example for each dataset) and the characteristic of each dataset. The simulated LST time series (Y_t), trend (T_t), seasonality (S_t), and remainder (e_t) are displayed as black dots; the simulated abrupt changes are displayed as red vertical lines. (For interpretation of the references to colour in this figure legend, the reader is referred to the web version of this article.)

magnitudes (−5–10 K), and different trend slopes after the abrupt change. A total of 1296 cases were simulated in dataset 2.

(3) Dataset 3: two abrupt changes were set in the trend component of the basic time series to assess the detection accuracy for multiple abrupt changes in trend. Different timing intervals between two abrupt changes were included, and a total of 648 cases were generated.

(4) Dataset 4: one seasonal abrupt change was simulated by changing the harmonic parameters (order, amplitude, and phase) after the abrupt change. This dataset with 297 cases was used to examine the detection accuracy of seasonal abrupt changes.

(5) Dataset 5: a total of 324 cases generated by setting two seasonal abrupt changes with distinct timing intervals were used to examine the feasibility of change detection methods on frequent seasonal changes.

(6) Dataset 6: a total of 1783 cases with one trend abrupt change and one seasonal abrupt change were generated by combining datasets 2 and 4 to evaluate the detection accuracy when both trend and seasonal abrupt changes were present.

3.2. MODIS LST time series

20 years LST time series from 2000 to 2021 with significant disturbances distributed around the world were sampled to test the performance of the change detection method on real LST data. First, we analyzed the global extreme weather event map from the early 2000s (https://www.carbonbrief.org/) and the global LCC maps produced by Estel et al. (2015); Hansen et al. (2013); Lark et al. (2020), Liu et al. (2014), and Song et al. (2018), and the MODIS yearly global land cover (LC) map (i.e., MCD12Q1, https://lpdaac.usgs.gov/products/mcd12q1v006/) coupled with time-series high-spatial-resolution images from Google Earth. From these data, we identified 22 sites where 33 significant disturbances have occurred, including 15 LCC events, such as deforestation with LC changing from forest to savannas (SAV), agricultural expansion with LC changing from barren (BAR) to cropland (CRO), farmland abandonment with LC changing from CRO to SAV, urbanization with LC changing from grassland (GRA) to urban and built-up land (UBL), forest gain or loss with forest cover change, 7 wildfires, 6 heatwaves, and 5 cold spells (hereafter referred to as cold). Second, MODIS 8-day composited LST data (MOD11A2, https://lpdaac.usgs.gov/products/mod11a2v006/) from 2000 to 2021 at these sites were downloaded. These time series can not only characterize detailed LST changes but also eliminate spikes caused by residual clouds, snow, smoke, or shadows. Fig. 6 shows the distribution of these sites. Table 3 provides detailed information about these sites and their disturbances.

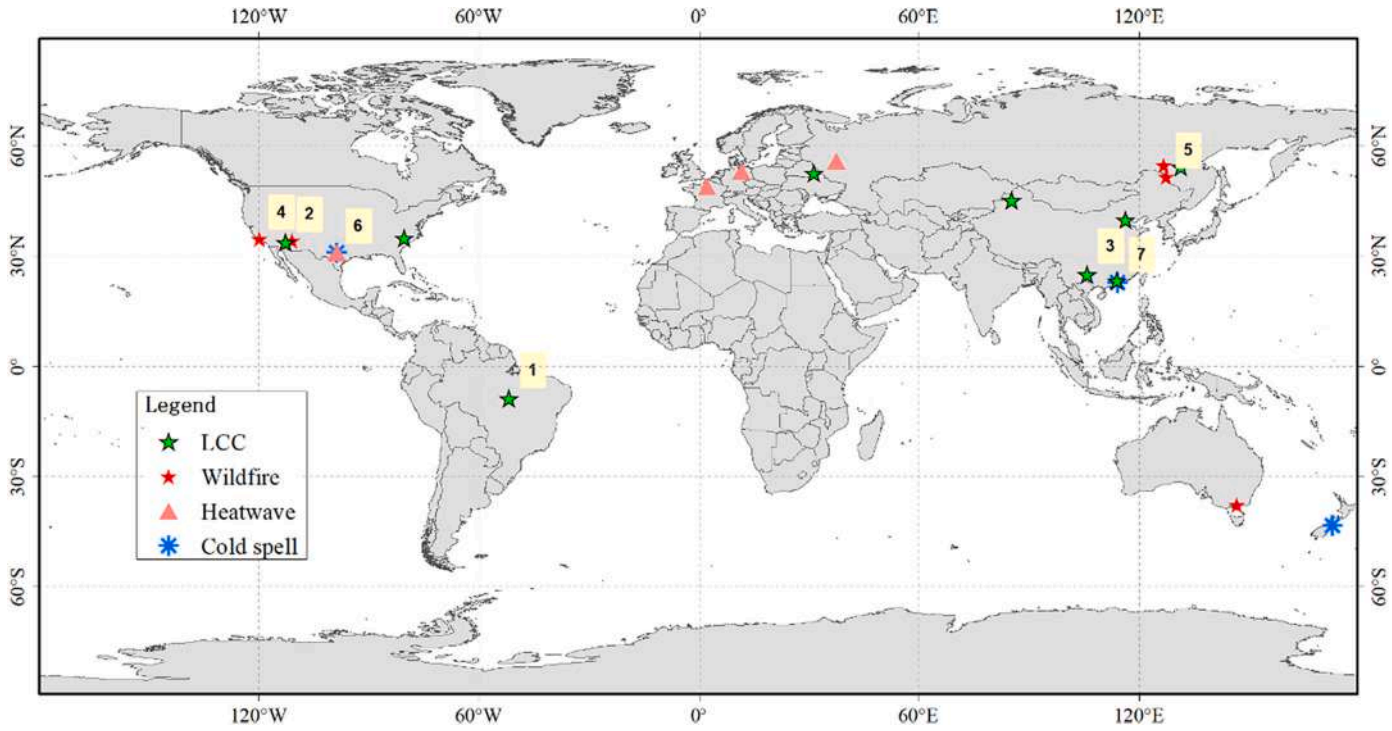

Fig. 6. Geolocations of 22 sites where known disturbances have occurred, including land cover change (LCC), wildfires, heatwaves, and cold spells. Seven sample sites (shown as yellow boxes) were selected to display the performance of the three methods. (For interpretation of the references to colour in this figure legend, the reader is referred to the web version of this article.)

4. Design of the comparison and criteria

When performing DBEST, BFAST, and BEAST, the related parameters should be defined. We first set common parameters including the maximum number of breakpoints in trend (m) for all three methods, maximum numbers of breakpoints in the seasonality (q), and minimum separation interval (ϕ) in BFAST and BEAST. We chose $m = q = 3$ to detect the first three significant abrupt changes in each component. ϕ was set to half of a year to test the applicability of the method to frequently disturbed data. This means that the minimum interval between the two breakpoints was half of a year, and the breakpoints were more than half of a year apart from the start and end of the time series. The parameters unique to each method were defined as follows.

DBEST was designed for NDVI time series (Jamali et al., 2015), therefore, to provide a reference for the definition of the level-shift thresholds (θ_1 and θ_2) and duration threshold (D), the min-max normalization strategy was used to normalize the LST data. Following the recommendation of Jamali et al. (2015), we set $\theta_1 = 0.1$, $\theta_2 = 0.2$ and $D = 2$ years to examine the major discontinuities in the LST series. Additionally, the missing data in the LST time series were filled using linear interpolation because DBEST cannot deal with irregularly spaced data series. Linear interpolation estimates each missing value based on the two adjacent data points. The R package of DBEST in the "change detection" mode was used to perform DBEST (https://github.com/HristoTomov/DBEST). Similarly, the missing LST data in the LST time series were filled for BFAST. The maximum number of iterations was set to five to achieve convergent results while reducing the computational cost (Awty-Carroll et al., 2019). The R package of BFAST was used in this study (https://github.com/bfast2/bfast). For BEAST, the maximum seasonal harmonic order was set to 3, which is in line with the setting in BFAST. In addition, the recommended sample number (i.e., 10,000) was used to achieve convergence in BEAST. BEAST is available as a R package and a MATLAB code, and the latter was employed in this study (https://github.com/zhaokg/Rbeast).

The performance of the change detection methods was evaluated from the following two aspects:

(1) Detection accuracy of abrupt changes. If the simulated dataset did not contain abrupt changes, the commission error (calculated by dividing the number of false detections by the total number of datasets) was employed to compare the three methods; otherwise, the F1 score (F1, Eq. (6)), calculated based on the user's accuracy (UA) and producer's accuracy (PA), and the mean absolute error (MAE) of the coordinate differences (δt) (Eq. (7)) were employed to assess the detection accuracy of abrupt changes (Chinchor, 1992). For the three methods, a breakpoint detected within half a period of the actual breakpoint (i.e., the simulated breakpoint in the simulated data) was determined to be a correct detection; otherwise, it was defined as a false detection.

$$F1 = 2 \times \frac{PA \times UA}{PA + UA}, \quad PA = \frac{TD}{TN}, UA = \frac{TD}{DN} \tag{6}$$

where PA is calculated as the number of correct detections (TD) divided by the number of reference breakpoints (TN), and UA is calculated as TD divided by the total number of detections (DN). The highest possible value of F1 is 1.0, indicating perfect PA and UA, and the lowest possible value is 0 if either the PA or the UA is zero.

$$MAE_{\delta t} = \frac{\sum_{c=1}^{O} \delta t_c}{O}, \delta t_c = \left| t_{ref} - \hat{t} \right|_c \tag{7}$$

where O is the number of breakpoints, t_{ref} is the timing coordinate of the actual breakpoint, and $\hat{t}$ is the timing coordinate of the detected breakpoint. $MAE\_\delta t$ directly measures the closeness of the detected breakpoint to the actual breakpoint. $MAE\_\delta t$ close to zero represents a more accurate detection.

For MODIS LST time series, owing to the small amount of data and the unknown underlying disturbances, the ability of the change detection method to detect disturbances was evaluated by comparing the number of correct detections. Considering the complexity of

Table 3
Details of 22 sites where known disturbances have occurred. Eight land cover types were involved, including evergreen broadleaf forest (EBF), savannas (SAV), grassland (GRA), shrubland (SHR), urban and built-up land (UBL), mixed forests (MF), barren (BAR), cropland (CRO), and woody savannas (WSAV).

Site	Disturbance	Geographical location		LC	Location
		longitudes (°)	latitude (°)		
1*	deforestation	−51.68	−8.92	EBF-SAV-GRA	Amazon rainforest in Brazil
2*	urbanization	−112.44	33.63	SHR-UBL	Southwest USA
3*	forest gain and forest loss	105.80	24.87	SAV-EBF-MF	South China
4*	wildfire	−119.59	34.64	SAV-GRA-SAV	California, USA
5*	wildfire	127.42	51.49	MF-SAV	Northeast China
6*	heatwave and cold spell	−98.67	30.75	UBL	Southwest USA
7*	cold spell	114.04	22.63	UBL	South China
8	deforestation	−46.26	−1.62	EBF-SAV	Amazon rainforest in Brazil
9	agricultural expansion	85.31	45.09	BAR-CRO	Xinjiang in China
10	agricultural expansion	−80.30	34.82	SAV-CRO	Southeast USA
11	farmland abandonment	31.43	52.54	CRO-MF	Eastern Europe
12	urbanization	113.93	23.16	CRO-UBL	South China
13	urbanization	116.27	39.74	CRO-UBL	North China
14	forest gain	131.36	54.12	SAV-DBF	Far Eastern Russia
15	wildfire	−110.63	34.20	SAV-WSAV	California, USA
16	wildfire	126.76	54.64	WSAV	Far Eastern Russia
17	wildfire	146.55	−37.79	EBF	Victoria, Australia
18	heatwave	11.86	53.08	UBL	Germany
19	heatwave	2.34	48.88	UBL	France
20	heatwave	37.62	55.77	UBL	Central Russia
21	heatwave and cold spell	−98.67	30.75	UBL	Southwest USA
22	cold spell	172.55	−43.48	UBL	New Zealand

* Seven sample sites in Fig. 6.

disturbances that occur in reality, a breakpoint detected within one year of the actual LCC disturbance or within six months of an actual small disturbance is determined as a correct detection.

(2) Component decomposition accuracy. In the simulated dataset, the root mean square errors (RMSE) values and correlation coefficient (R) values between each predicted and simulated (i.e., actual) component (i.e., trend and seasonality) were employed to measure the decomposition accuracy of each component. The RMSE of the predicted trend component was denoted as $RMSE_{T_t}$, and the RMSE of the predicted seasonality was denoted as $RMSE_{S_t}$.

The true trend and seasonality are not known in MODIS LST time series, so the RMSE between the sum of the predicted trend and seasonality and time-series observations ($RMSE_{T_t+S_t}$) was employed to measure the overall fitting accuracy of the $T_t + S_t$.

5. Comparison with simulated data

The computational costs of DBEST, BFAST, and BEAST were first compared. When these methods were run on a configuration using 12 cores, with 2.20GHz and 16-GB memory, the time required for each method to process 100 10-year time series with a temporal resolution of 8 days is 34.9 s, 3.7 s, and 10.8 s, respectively. BFAST showed the highest computational efficiency among the three methods. Although the computational cost of BEAST is larger than BFAST, it is acceptable and feasible in actual operation. The following section reports our assessment of the three methods from the following two aspects: abrupt change detection and component decomposition.

5.1. Detection accuracy of abrupt changes

Table 4 illustrates the F1 scores of the trend abrupt change detection using DBEST, BFAST, and BEAST, and the F1 scores of the seasonal abrupt change detection using BFAST and BEAST. BEAST exhibited the largest mean F1 of 0.83 and 0.95 for abrupt change detection in the two components, respectively. BFAST showed marginally higher F1 (mean value: 0.56) than DBEST (mean value: 0.37) for trend abrupt change detection. The F1 of trend abrupt changes detected by BEAST decreased by 0.04 when one seasonal abrupt change was added to the data (from dataset 2 to dataset 6), and the change in F1 of DBEST was −0.02, however, the F1 loss of BFAST was 0.32. This finding suggests that as the complexity of the data increases, BEAST and DBEST exhibited more stable F1 than BFAST, on the contrary, BFAST was ineffective for detecting trend abrupt changes when seasonal abrupt changes occur simultaneously.

For datasets 1, 4, and 5, no trend abrupt changes occurred, and the commission error of trend abrupt change detection was employed to evaluate the performance of the three methods. Similarly, the commission error of seasonal abrupt change detection was calculated for datasets 1, 2, and 3. As shown in Table 5, the smallest commission error was observed for BEAST, in which the greatest values were 25.9% and 24.8% in the two components, respectively. BFAST had a much lower commission error for seasonal abrupt changes detection than that of trend abrupt changes detection. In addition, the significant commission error of trend abrupt changes of BFAST on datasets 4 and 5 again suggested that BFAST has low robustness to data with high complexities. DBEST yielded the poorest accuracy, with false trend abrupt change detection observed in every simulation data.

To further explore the accuracy of the detected breakpoints, the mean absolute error of the coordinate differences ($MAE\_\delta t$, Eq. (7)) between the breakpoints detected by the three tested methods and the actual breakpoints were shown in Fig. 7. BEAST performed most effectively, with the smallest $MAE\_\delta t$ of <9 observations (<1/5 period) for trend breakpoints and <3 observations (less than one month) for seasonal breakpoints. For trend abrupt detection, BFAST yielded results comparable to those of BEAST when only trend abrupt changes occurred, that is, in datasets 2 and 3. However, when seasonal abrupt changes occurred (i.e., in dataset 6), the $MAE\_\delta t$ of breakpoints detected by BFAST in trend increased significantly, with values of 62 observations. The $MAE\_\delta t$ of seasonal breakpoints detected by BFAST was <9 observations, so it can be used as an alternative method for detecting seasonal abrupt changes. The performance of DBEST remains the worst, with a mean $MAE\_\delta t$ of 28 observations.

In addition, Fig. 8 illustrated the detection results of the three methods on six typical simulated time series displayed in Fig. 5. It demonstrated that both BEAST and BFAST detected eight true breakpoints with MAE_δt values of 0 observation. The difference is that BEAST detected 9 breakpoints, while BFAST detected 20 breakpoints, which means BEAST had a smaller commission error than BFAST. DBEST detected four correct breakpoints among 15 detections with MAE_δt of 10 observations. Moreover, the components decomposed by DBEST contain more redundant information than the other two methods.

5.2. Component decomposition accuracy

Fig. 9 displays the RMSEs of the trend and seasonality decomposed by the three tested methods and the correlation coefficients between the

Table 4
Number of correct detections (Correct), all detections (All), and F1 scores of abrupt change detection in trend (T_t) and seasonality (S_t) for DBEST, BFAST, and BEAST in different simulated datasets.

Component with abrupt changes	No. of datasets.	Number of true breakpoints	DBEST			BFAST			BEAST		
			Correct	All	F1	Correct	All	F1	Correct	All	F1
T_t	2	1296	799	3564	**0.33**	1055	2272	**0.59**	1081	1310	**0.83**
	3	2124	1078	2767	**0.44**	1864	2481	**0.81**	1848	2077	**0.88**
	6	1782	1204	5037	**0.35**	804	4049	**0.28**	1386	1738	**0.79**
					0.37*			**0.56***			**0.83***
S_t	4	297				175	585	**0.40**	297	334	**0.94**
	5	648				537	807	**0.74**	623	664	**0.95**
	6	1782				1042	3049	**0.43**	1782	1976	**0.95**
								0.52*			**0.95***

* Mean values of F1 score.

Table 5
Number of false detections and commission errors of DBEST, BFAST, and BEAST for different simulated datasets without abrupt changes in trend (T_t) or seasonality (S_t).

Component without abrupt changes	No. of datasets	Number of cases	DBEST		BFAST		BEAST	
			False detections	Commission error (%)	False detections	Commission error (%)	False detections	Commission error (%)
T_t	1	648	1828	**282.1**	688	**106.2**	168	**25.9**
	4	297	822	**276.8**	585	**197.0**	37	**12.5**
	5	324	864	**266.7**	972	**300.0**	46	**14.2**
S_t	1	648			240	**37.0**	85	**13.1**
	2	1296			636	**49.1**	227	**17.5**
	3	1062			657	**61.9**	263	**24.8**

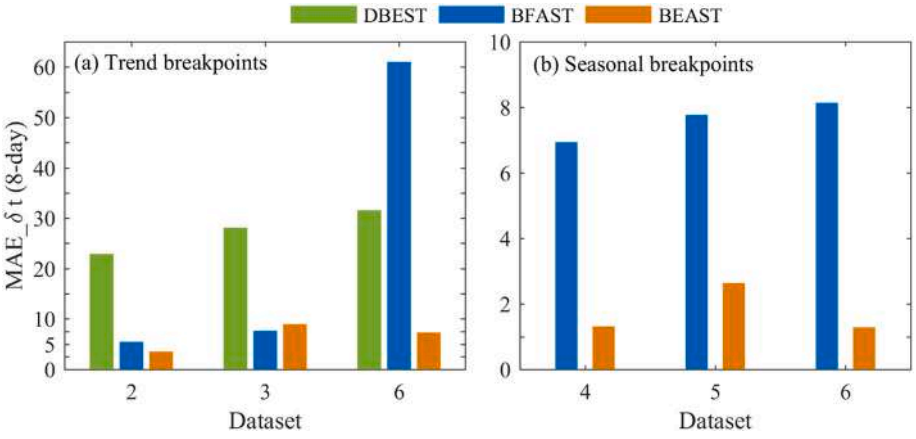

Fig. 7. Mean absolute error of the coordinate differences (*MAE_δt*, Eq. (7)) between the breakpoints detected by DBEST, BFAST, and BEAST in (a) trend and (b) seasonality and the actual breakpoints.

actual and predicted components. BEAST decomposed time-series data with the highest fidelity, with mean RMSEs of 0.28 K and 0.27 K and mean R values of 0.90 and 0.99 for T_t and S_t, respectively. The next best decomposition was achieved by DBEST, with mean RMSEs of 0.64 K and 1.37 K and mean R values of 0.78 and 0.98 for the two components, respectively. BFAST showed the worst performance, with mean RMSEs of 1.34 K and 1.46 K and mean R values of 0.69 and 0.97, respectively. For datasets 1, 2, and 3, BFAST showed better performance than DBEST; however, BFAST exhibited larger RMSEs and smaller R values than DBEST for datasets 4, 5, and 6. This reduction in accuracy suggests that BFAST is inefficient for data with high seasonal variation. Additionally, it is interesting to note that the R values of the trend components were smaller than those of the seasonal components. This is mainly because the high seasonality of the LST produces a mirage correlation between the predicted and actual seasonal components (Deyle et al., 2016).

6. Improvement of BEAST

Although the accuracy of BEAST was significantly higher than that of the other change detection methods, this method exhibited non-negligible commission errors for trend breakpoint detection (mean value on simulated data: 18.6%). To accurately describe long-term variations in LST, it is necessary to further eliminate false breakpoints detected by BEAST.

True abrupt changes are always accompanied by sudden increases or decreases in T_t or significant changes in the slope of T_t. Meanwhile, BEAST outputs the occurrence probability of the breakpoint and remainder (e_t). A high probability indicates a high likelihood of the breakpoint. The abnormal e_t tends to occur when true abrupt change happens (Fig. 8). Based on these facts, four features were first selected to describe the above characteristics (Fig. 10), including 1) the change magnitude of trend abrupt changes (Δ trend), 2) the changes in the slope of the trend before and after the abrupt change occurred, measured by the angle between the two trends (Angle), 3) the occurrence probability

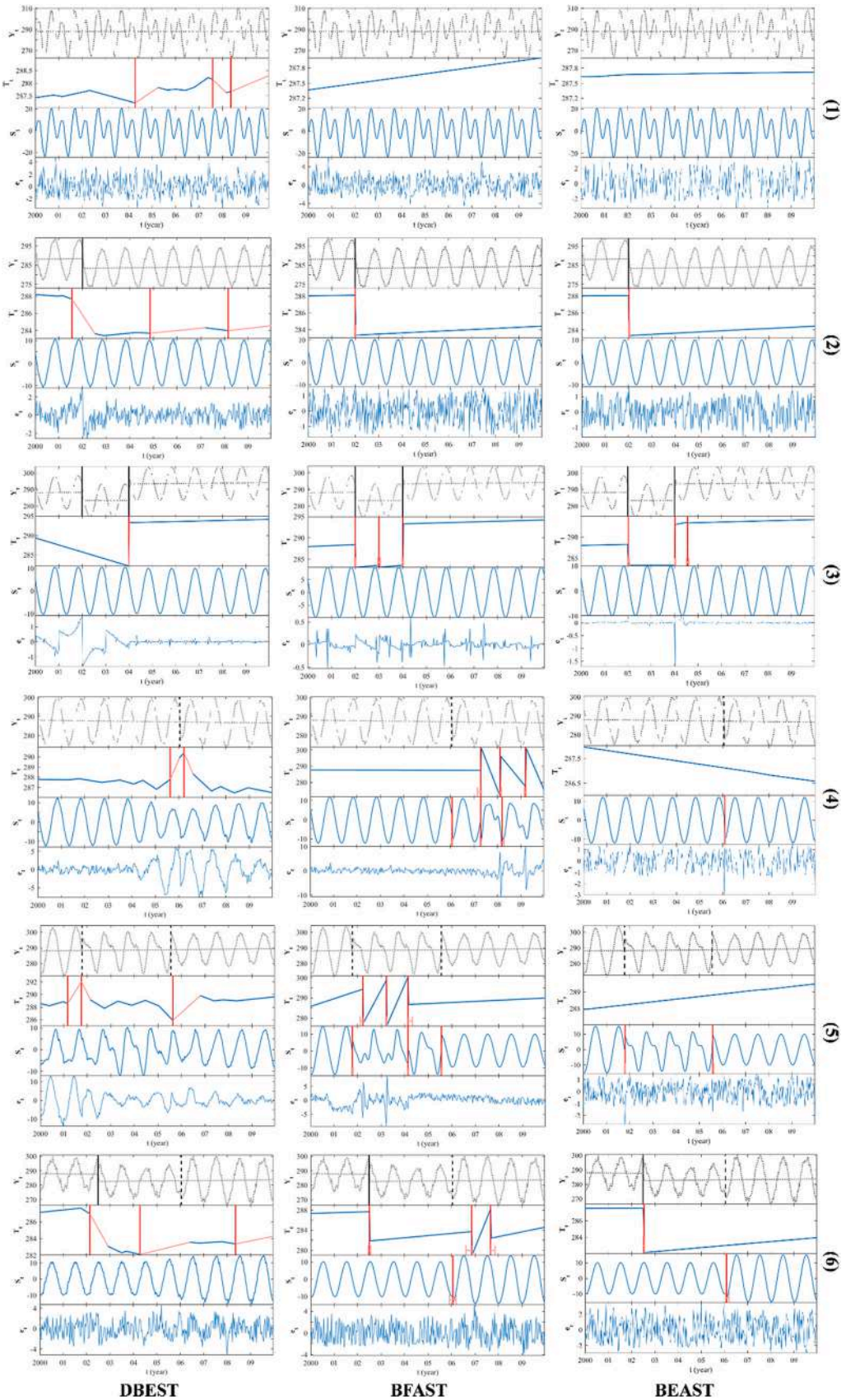

Fig. 8. Change detection results of DBEST, BFAST, and BEAST using six simulated LST time series displayed in Fig. 5. The simulated time series (Y_t) and trend were displayed as black dots; The simulated abrupt changes in trend (vertical black line) and seasonality (vertical black dotted line) were also shown in the first row of each subgraph; The decomposed trend (T_t), seasonality (S_t), and remainder (e_t) are displayed as blue lines; the detected abrupt changes and their confidence intervals are shown as vertical red lines. (For interpretation of the references to colour in this figure legend, the reader is referred to the web version of this article.)

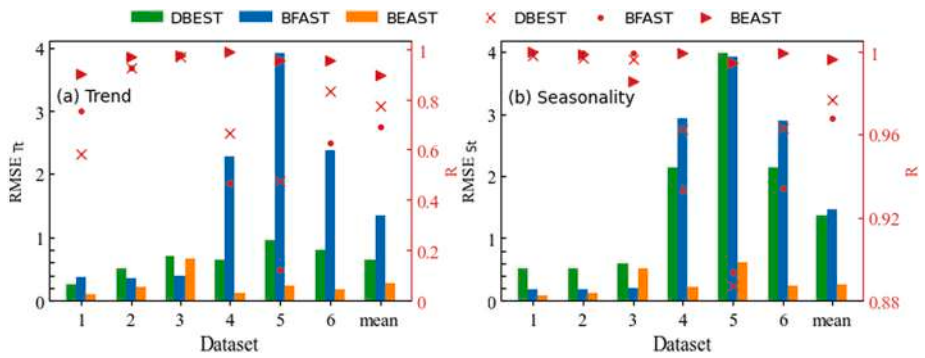

Fig. 9. The RMSEs of the decomposed trend (a, $RMSE_{T_t}$) and seasonality (b, $RMSE_{S_t}$) using DBEST, BFAST, and BEAST, and the correlation coefficients (R) between the actual and the predicted components.

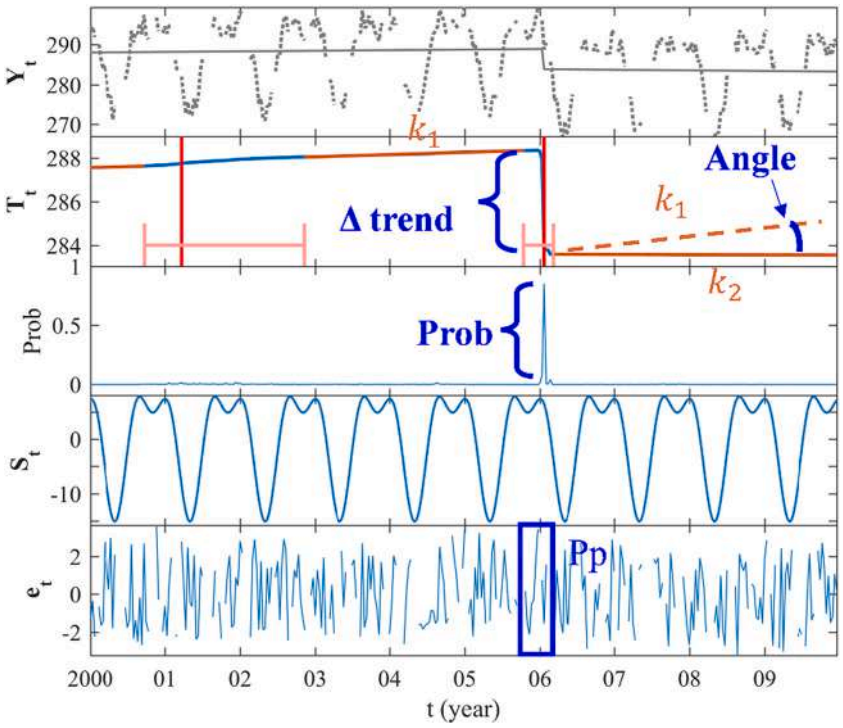

Fig. 10. Illustration of the four features used to eliminate false breakpoints, including change in magnitude of trend abrupt changes (Δtrend), the angle between two trends before and after the abrupt change occurred (Angle), the occurrence probability of the detected breakpoints (Prob), and the proportion of abnormal remainders in the confidence interval of the abrupt change (Pp). k_1 and k_2 are slopes of the two trends before and after the abrupt change obtained based on linear fitting.

of the detected breakpoints (Prob), and 4) the proportion of abnormal remainders in the confidence interval of the abrupt change (Pp). The identification of the abnormal remainders followed by Zhu and Woodcock (2014): an abnormal remainder will be detected if the remainder is larger than three times the $RMSE_{T_t+S_t}$. Then, we used four criteria to judge the false breakpoints: Δ trend < T1 and Angle < T2 and

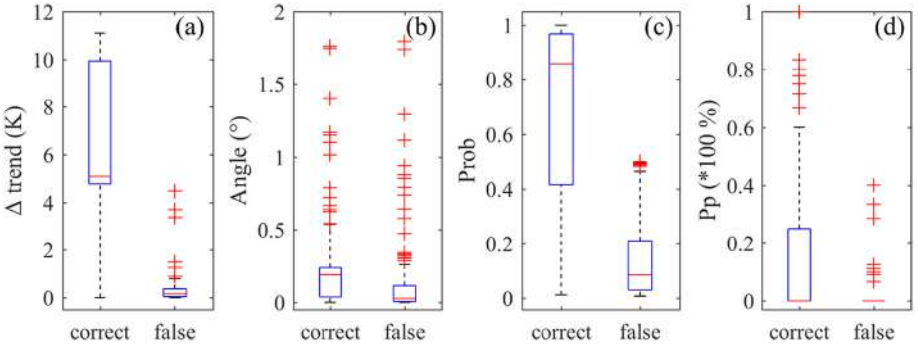

Fig. 11. Boxplot of (a) Δtrend, (b) Angle, (c) Prob, and (d) Pp for correct and false breakpoints detected by BEAST in simulated dataset 3. The top and bottom whiskers are the highest and lowest value, respectively, excluding outliers; the top and bottom of the box are the 75th and 25th percentiles of the statistical dataset; the band inside each box denotes the median value for each feature; and outliers were plotted individually using the '+' marker symbol.

Prob < T3 and Pp < T4. To determine the optimal thresholds (T1, T2, T3, and T4), the following two steps were conducted.

First, a series of threshold candidates were designed based on dataset 3. As shown in Fig. 11, significant differences in Δ*trend*, *Angle*, *Prob*, *and Pp* were found between correct and false breakpoints: most false breakpoints had Δ trend of <1 K, Angle of <0.3°, Prob of <0.5, and Pp close to 0. Based on these differences, T1, T2 and T4 were determined by traversing our designed potential threshold combinations: four Δ*trend* thresholds (0.5 K, 1 K, 2 K, 5 K), three Angle thresholds (0.1°, 0.5°, 1°), and four Proportion (Pp) thresholds (1%, 5%, 10%, 50%). T3 was arbitrarily set as 0.5.

Second, the F1 score and number of correct breakpoints (TD) for each candidate combination were calculated and the optimal threshold combination with the highest accuracy was obtained. As shown in Fig. 12, BEAST achieved higher accuracy after eliminating false breakpoints. The mean F1 increased when the Δtrend threshold ranged from 0.5 K to 2 K. When the Pp threshold was <5%, a higher Angle threshold led to a higher F1. However, a higher F1 may result in a smaller TD. To obtain a balance between F1 and TD and avoid excessively harsh threshold conditions, we chose Prob ≤0.5, Δtrend ≤1 K, Angle ≤1°, and Pp ≤ 1% to eliminate false breakpoints.

To examine the applicability of the optimal thresholds determined by dataset 3 to other datasets, Tables 6 and 7 showed the changes in the accuracy for six simulated datasets after eliminating false breakpoints using these thresholds. Here, the elimination rate was defined by the percentage of eliminated false breakpoints against all detected false breakpoints. In dataset 3, the elimination rate was 88%. Although the number of correct breakpoints reduced marginally, the F1 values increased by 0.04 and the UA increased remarkably was 10%, which determines the reliability of the interpretation of the detected data and is more critical to the analyst than the producer's accuracy (PA) (Patel and Kaushal, 2010). When applying the optimal thresholds to other datasets (1,2,4,5, and 6), the mean value of the elimination rate was 77% (datasets 1,2,4,5, and 6), the F1 increment was 0.05 (datasets 2 and 6), and the user accuracy increment was 16% (datasets 2 and 6). These significant improvements in accuracy demonstrated the applicability of the optimal threshold to different datasets.

7. Application to MODIS LST time series

7.1. Preliminary results

DBEST, BFAST, BEAST, and the improved BEAST were used to examine the applicability of change detection methods to MODIS LST time series. In the improved BEAST, the thresholds recommended in Section 6 (i.e., Prob ≤0.5, Δtrend ≤1 K, Angle ≤1°, and Pp ≤ 1%) were employed to eliminate false breakpoints in all MODIS LST time series. Additionally, we used a minimum of two years of data (i.e., 92 observations in LST time series) between successive LCC detections to avoid having data with high variability, according to the recommendations of Bai and Perron (2003). Specifically, we merged two adjacent breakpoints with a stable period of less than two years by keeping the breakpoints with higher Prob and eliminated the breakpoints that were less than two years from the start or the end of the time series. After eliminating the false trend breakpoints, the trend between the retained breakpoints was refitted by the linear function, and then the remainder was updated.

Table 8 lists the disturbance detection results of the four methods at 22 sites. For LCC detection, BEAST gave the best performance with the most correct detections of 13 in 15 true disturbances (86.7%), followed by DBEST (9) and BFAST (7). For small disturbances (e.g., wildfires, heatwaves, and cold) detection, all three methods exhibited poor detection efficiency with correct detections of <9 in 18 true disturbances (50%). The improved BEAST eliminated 15 "false" breakpoints, which can be considered as useless breakpoints while sacrificing one true breakpoint. As seen from the accuracy of fitting MODIS LST time series with $T_t + S_t$ decomposed by the four methods at 22 sites (Fig. 13), the $RMSE_{T_t+S_t}$ of DBEST was a little lower than that of the other three methods. This is because the trend and seasonality decomposed by DBEST tend to contain many meaningless detailed fluctuations and turning points, resulting in the lower $RMSE_{T_t+S_t}$ for fitting the MODIS LST time series. It should be emphasized that the $RMSE_{T_t+S_t}$ only indicates the overall accuracy of fitting the LST time series, not the accuracy of component decomposition (T_t and S_t) and abrupt change detection, and good overall accuracy does not imply high accuracy of component decomposition and abrupt change detection. In fact, as shown in Fig. 9 and Table 8, the performance of DBEST for component decomposition and abrupt change detection was lower than that of BFAST and BEAST.

To further compare the performance of the four methods in detecting

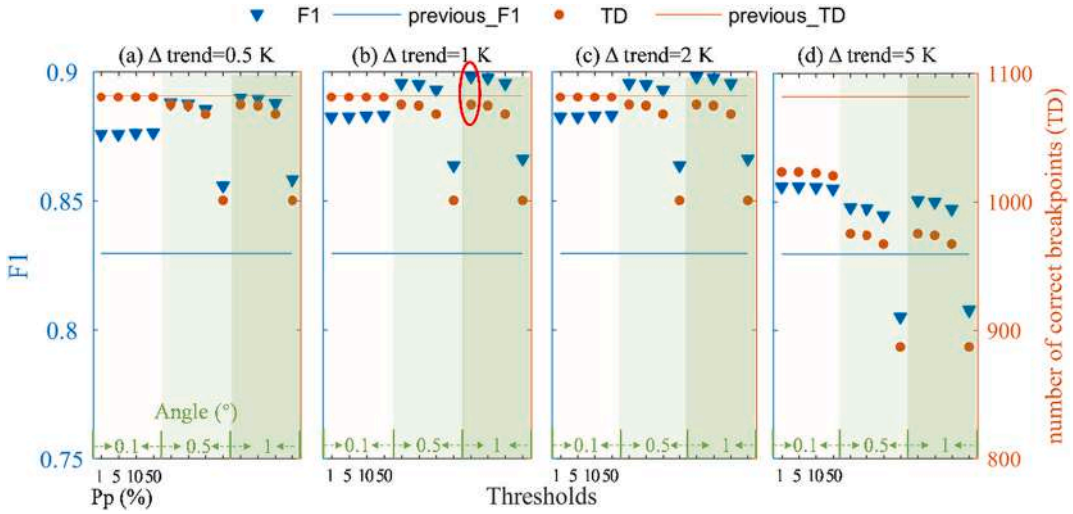

Fig. 12. Changes in F1 score and number of correct breakpoints (TD) under different threshold groups, including four Δ trend thresholds (0.5 K (a), 1 K (b), 2 K (c), 5 K (d)), three Angle thresholds (0.1°, 0.5°, 1°), and four Proportion (Pp) thresholds (1%, 5%, 10%, 50%). The optimal thresholds correspond to the red ellipse. (For interpretation of the references to colour in this figure legend, the reader is referred to the web version of this article.)

Table 6
Changes in F1, UA, PA, number of correct detections, all detections, and false detections before and after eliminating false breakpoints and the elimination rate of false detections defined as the percentage of eliminated false breakpoints against all detected false breakpoints.

No. of datasets	Number of true breakpoints		F1	UA (%)	PA (%)	Correct detection	All detection	False detection	Elimination rate (%)
2	1296	Before	0.83	82.5	83.4	1081	1310	229	90.4
		After	**0.90**	**98.0**	**82.9**	**1074**	**1096**	**22**	
3	2124	Before	0.88	89.0	87.0	1848	2077	229	87.8
		After	**0.91**	**98.5**	**84.1**	**1786**	**1814**	**28**	
6	1782	Before	0.79	79.7	77.8	1386	1738	352	86.4
		After	**0.82**	**96.4**	**71.6**	**1276**	**1324**	**48**	

Table 7
Changes in commission error and number of false detections before and after eliminating false breakpoints and the elimination rate of false detections defined as the percentage of eliminated false breakpoints against all detected false breakpoints.

No. of datasets	Number of cases		Commission error (%)	False detection	Elimination rate (%)
1	648	Before	25.9	168	93.5
		After	**1.7**	**11**	
4	297	Before	12.5	37	62.2
		After	**4.7**	**14**	
5	324	Before	14.2	46	54.3
		After	**6.5**	**21**	

different types of abrupt events in detail, we displayed the detection results of these methods at seven sampled sites with LCC and low-magnitude disturbances (e.g., wildfires, heatwaves, and cold) in the following sections. The detection results of the other 15 sampled sites were given in supplementary data (Fig. S1- S7). The high-resolution image sequence associated with LCC and the corresponding detection results were illustrated in Figs. 14 and 15, respectively. Similarly, Figs. 16 and Fig. 17 show the results for wildfires, and Fig. 18 shows the results for heatwaves and cold.

(1) LCC detection results

Fig. 14 is based on MODIS LST data with three different types of LCC, including deforestation, urbanization, and forest gain and loss.

At site 1, the forest in the selected pixel (green box) was cut down in 2008, and the vegetation was further reduced in 2011. In 2018, this pixel had the lowest vegetation coverage. Therefore, the LC changed from evergreen broadleaf forest (EBF) to SAV in 2008 and changed from SAV to GRA in 2018 (Fig. 14). As shown in Fig. 15, BEAST unveiled three true change points accurately: the LCC in 2008 caused a sudden increase in the trend and a sudden increase in the amplitude of the seasonality, further deforestation in 2011 led to an abrupt increase in the trend, and the LCC in 2018 also caused an abrupt change in seasonality. However, BEAST exhibited two redundant breakpoints, which were eliminated by the improved BEAST. DBEST detected these three abrupt changes in trend, however, it ignored the seasonal changes caused by the LCC. BFAST showed the worst performance, detecting only one true abrupt change and ignoring the seasonal changes, which reveals that BFAST is less sensitive to seasonal abrupt changes. All three methods can unveil the warming trend caused by deforestation. However, several differences were observed: the trend in the confidence interval corresponding to the detected abrupt change in BEAST uncovered the deforestation process with high fidelity; although DBEST also reflected the change process using the trend during the change duration, its least generalized trend with all possible details would complicate the subsequent LST change analysis, while the abrupt change detected by BFAST was transient and could not reveal the change process.

Site 2 demonstrates the evolution of urbanization (Fig. 14). In the selected pixel, the vegetation was cleared in 2004, and buildings were constructed during 2005–2006. Correspondingly, the LC changed from SHR to BAR in 2004 and changed from BAR to UBL during 2005–2006. As seen in Fig. 15, BEAST detected these two changes, including trend abrupt increase and seasonal abrupt change. The improved BEAST eliminated the first abundant trend breakpoint. BFAST also detected these two abrupt changes but ignored the seasonal abrupt change, which again suggested its ineffectiveness in seasonal abrupt change detection. DBEST missed the significant change during 2005–2006.

In site 3, the LC of the selected pixel changed from SAV to EBF around 2005 due to the "Grain for Green" project, and since 2017, part of the forest in the pixel has been felled, resulting in the LC changing from EBF to mixed forest (MF) (Fig. 14). As shown in Fig. 15, BEAST captured the forest gain process but missed the forest loss change, while BFAST and DBEST ignored the two forest cover changes. Additionally,

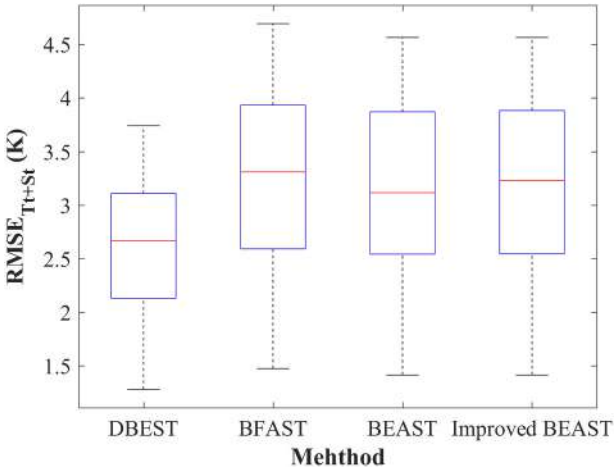

Fig. 13. RMSE boxplot of the sum of trend and seasonality ($RMSE_{T_t+S_t}$) decomposed by DBEST, BFAST, BEAST, and the improved BEAST using MODIS LST time series.

Table 8
Number of correct breakpoint detections (Correct) and all detections (All) in DBEST, BFAST, and BEAST based on MODIS LST time series at 22 sites.

Events	Number of true breakpoints	DBEST		BFAST		BEAST		Improved BEAST	
		All	**Correct**	All	**Correct**	All	**Correct**	All	**Correct**
LCC	**15**	30	**9**	22	**7**	25	**13**	14	**12**
Wildfire	**7**	15	**4**	14	**4**	14	**4**	13	**4**
Heatwave	**6**	12	**1**	10	**1**	8	**2**	6	**2**
Cold	**5**	9	**3**	6	**2**	6	**2**	5	**2**

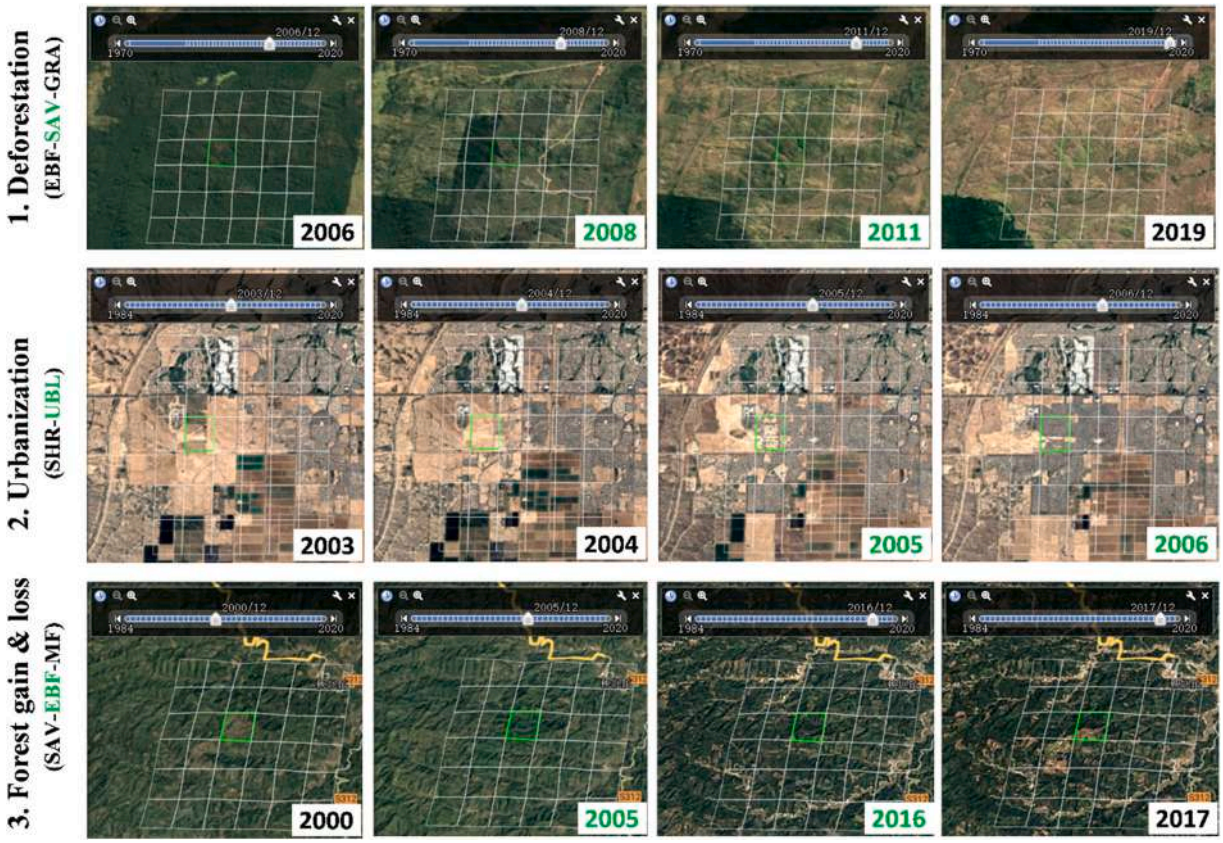

Fig. 14. Evolution of the land cover change (LCC) at sites 1, 2, and 3. High spatial resolution image sequences are from Google Earth. MODIS pixels are shown in white boxes and the selected pixels are shown in the green box. The green text represents the land cover type after the LCC and its corresponding year. Site 1 highlights deforestation playing out after 2008 in the Brazilian Amazon. Site 2 is an example of urbanization in Arizona, U.S. Site 3 displays the processes of forest gain and loss in Guizhou province, China. (For interpretation of the references to colour in this figure legend, the reader is referred to the web version of this article.)

these two methods exhibited a deviant trend dynamic around 2012 that divorced from the true smoothing trend dynamic. These results may have occurred because linear interpolation provides poor estimations when time-series data have long-lasting continuous missing and outliers (Zhang et al., 2019). A significant cooling effect of forest gain was observed by BEAST and DBEST.

(2) Low-magnitude disturbance detection results

Fig. 16 shows the performance of the three test methods in fire detection. At site 4, a month-old wildfire burning through SAV lands led to the LC changing from SAV to GRA. All three methods detected the wildfire and depicted the temperature rise dynamic when the fire occurred (Fig. 17). However, DBEST detected fire with the largest timing error. At site 5, two wildfires that lasted 11 days and 18 days occurred in 2002 and 2016, respectively, and the second fire caused forest loss (i.e., the LC changing from MF to SAV) (Fig. 16). However, all three methods ignored the two fires (Fig. 17). This may be attributed to the low intensity and the short duration of the fire, which displays as a few outliers in the time series. The same phenomenon is observed in Fig. 18. At site 6, a severe storm (lasting for 4 days), a cold spell (lasting for more than two weeks), and a heatwave (lasting for more than two months) occurred in April 2007, February 2010, and the summer of 2011, respectively; all three methods detected these disturbances. However, at site 7, two cold spells struck much of south China, and all three methods ignored these two disturbances, producing outliers in the remainder component. The improved BEAST eliminated the "false" breakpoints detected at sites 5 and 7, leading to a more generalized trend output.

7.2. Application of the improved BEAST with LST data

As mentioned above, the improved BEAST is likely to ignore subtle changes with small change magnitudes or short durations: the average omission errors calculated using simulated data for abrupt changes in trend and seasonality were 17.3% and 1.3%, respectively, and >50% of low-magnitude real disturbances will be likely missed. If a disturbance has a short duration (i.e., less than the temporal resolution of the data) or low intensity, the disturbance appears as an abnormal residual in the output. Therefore, it is necessary to use the time series at appropriate time intervals to detect subtle changes without losing the generality of the components.

In addition, the harmonic function used to estimate the seasonality can be considered part of the ATC model, and changes in the model parameters (e.g., mean temperature, amplitude, and phase) are related to changes in climate and atmospheric component concentrations (Bechtel, 2015; Stine et al., 2009; Thomson, 1995; Weng et al., 2004). However, a high-order harmonic generates multiple sets of these three parameters, which makes the physical meaning of these parameters unclear. Therefore, it is necessary to determine the optimal harmonic order to balance the fitting accuracy of the seasonality and the number of model parameters. Harmonic functions with different orders were applied to de-trended time series, calculated by subtracting the trend decomposed by BEAST from the original MODIS LST data. Fig. 19 shows the changes in the RMSE and R^2 of harmonic functions with different orders based on the data sampled at 20° E and 110° E longitudes (Lon). The result demonstrated that the 2nd harmonic achieved comparable RMSE and R^2 to the 3rd harmonic for all sampled time series. The fitting accuracy of the 2nd harmonic is higher than that of the 1st harmonic in the equatorial region (30° to −30° latitude (Lat)) and polar region (−90°

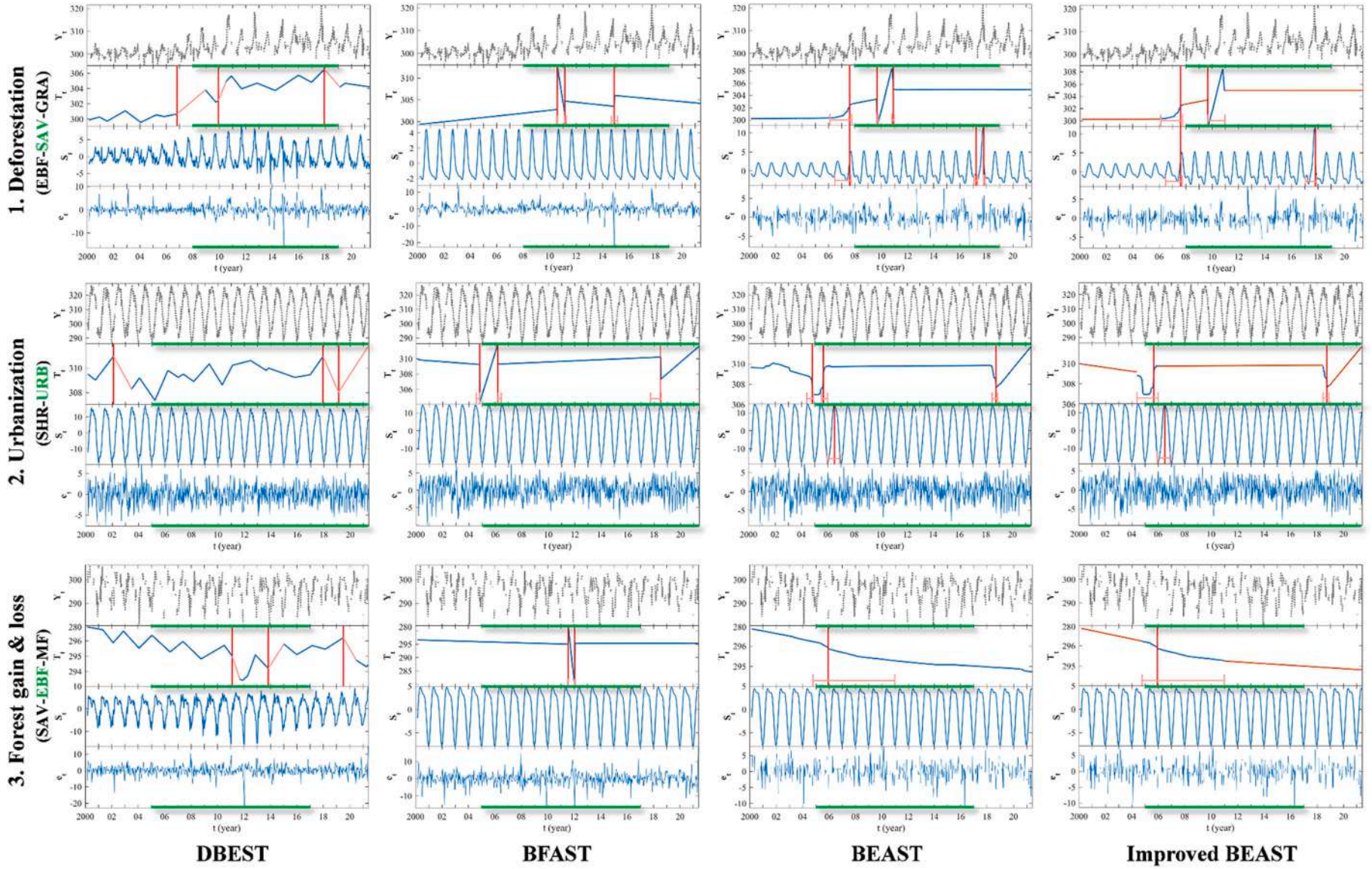

Fig. 15. Change detection results of DBEST, BFAST, BEAST, and the improved BEAST with known LCC disturbances, including deforestation with land cover changing from EBF to SAV and from SAV to GRA at site 1, urbanization (SHR-UBL) at site 2, and forest gain and loss (SAV-EBF-MF) at site 3. The time-series LST observations (Y_t) are displayed as grey dots; the decomposed trend (T_t), seasonality (S_t), and remainder (e_t) are displayed as blue lines; the refitting trend segments in the improved BEAST are displayed as red lines; the detected abrupt changes and their confidence intervals are shown as vertical red lines; and the land cover types after LCC are displayed in green. (For interpretation of the references to colour in this figure legend, the reader is referred to the web version of this article.)

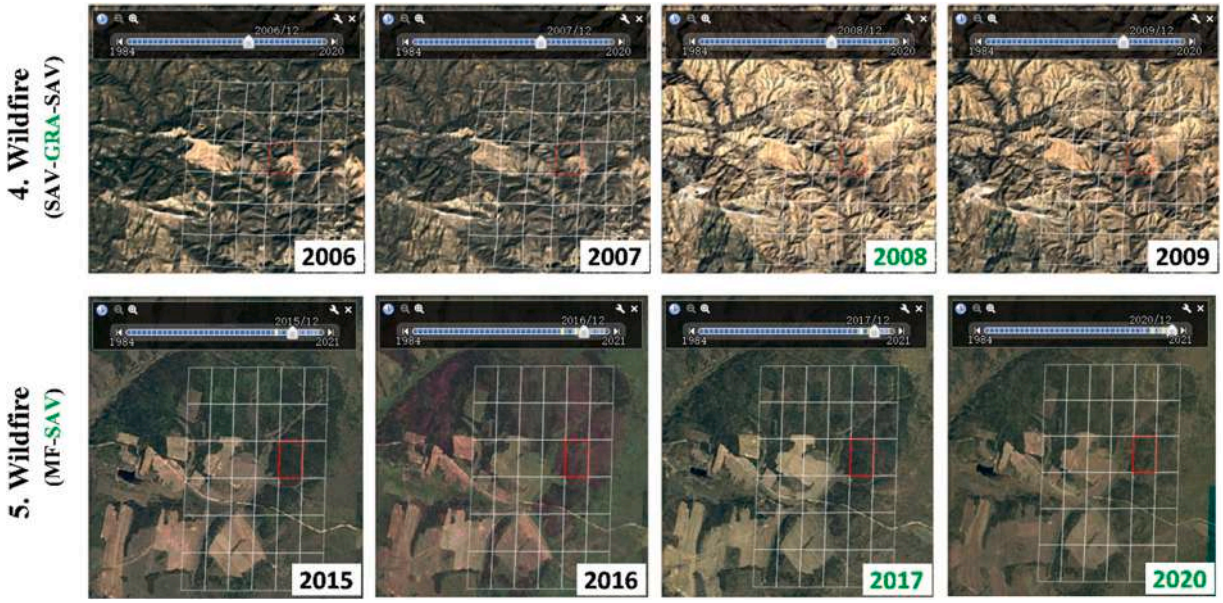

Fig. 16. Same as Fig. 14 but for wildfire. Sites 4 and 5 provide satellite views of the wildfire that occurred in California, the USA in 2007 and the wildfire that occurred in Amur Oblast, Russia in 2016, respectively.

to −70° and 70° to 90° Lat). It is interesting to note that all harmonics reached the lowest R^2 at Lat = 15° (Fig. 19b), but the RMSE at this latitude was lower than that of other latitudes (Fig. 19a). This result may have occurred because of the small amplitude (15 K) but the large temporal variation of LST in the equatorial regions. Similarly, compared with the equatorial region, LST exhibited a larger amplitude (40 K) but smaller variation in the Antarctic, which resulted in a larger RMSE (Fig. 19a) and a higher R^2 (Fig. 19b). These assessments suggest that when using the improved BEAST, the optimal value of the minimum seasonal harmonic order should be set to 1, and the maximum seasonal harmonic order should be set to 2.

8. Conclusion

Change detection methods are crucial for characterizing LST changes on multiple timescales, but until now, a systematic comparison among the proposed methods for analyzing LST data had not been performed. This study aims to evaluate the three commonly used methods, DBEST, BFAST, and BEAST, using simulated data with a wide range of change scenarios and MODIS LST time series with known disturbances. The results demonstrated the following:

(1) BEAST exhibited the highest detection accuracy for abrupt changes in both trend (F1 = 0.83) and seasonality (F1 = 0.95), and can characterize the process of abrupt changes. In addition, it can accurately decompose time-series data into trend and seasonality, with mean RMSE values of 0.28 K and 0.27 K, respectively. Additionally, when applied to the MODIS time series, BEAST detected LCC with a respectable success rate (13 in 15), and this high efficiency demonstrates the applicability of BEAST for real-world application. However, BEAST lacks sensitivity to subtle changes with non-negligible omission errors in simulated data (mean value of 16.9% for trend and seasonal abrupt changes) and with correct detections of <9 in 18 low-magnitude short-lived disturbances (e.g., wildfires, heatwaves, and cold spells)—some aspects that can be further improved in future algorithm implementation. Therefore, BEAST is most reliable if applied to detect changes with moderate to large magnitudes.

(2) BFAST demonstrated poorer performance than BEAST, with lower mean F1s of breakpoints (0.56 and 0.52 in trend and seasonality, respectively) and higher RMSEs of components (1.34 K and 1.46 K for the two components, respectively) in simulated data. This method appeared to be more affected by data complexities. Moreover, BFAST tends to detect incorrect trend dynamics when the time-series data have long-lasting missing. The above two limitations resulted in marginal efficiency for detecting true LCC (7 correct detections in 15 LCCs) and lower sensitivity to low-magnitude disturbances (7 correct detections in 18 low-magnitude disturbances). Additionally, extreme disturbance events tend to last for a period of time; however, the abrupt changes detected by BFAST cannot provide the details of the change process. The decomposed trends may not accurately reflect long-term temperature changes because BFAST does not eliminate disturbance periods when estimating the trend.

(3) The poorest accuracy was observed for DBEST in simulated LST data: the mean F1 was 0.37 and mean RMSEs of trend and seasonality were 0.64 K and 1.37 K, respectively. Similar to BFAST, DBEST also demonstrated a high sensitivity to long-lasting data and marginal efficiency for detecting true disturbances (9 correct detections in 15 LCCs and 8 correct detections in 18 low-magnitude disturbances). Additionally, the trend trajectory estimated by DBEST contains a quantity of non-essential change information, and it cannot detect seasonal abrupt changes.

To advance the analysis of the LST time series, we made improvements to BEAST by eliminating false breakpoints. Compared with BEAST, the user accuracy of the improved BEAST was significantly increased by 13.9% in the simulated data, resulting in an F1 increase of 0.04, and 15 (from a total of 53 detections) false breakpoints were eliminated in the MODIS LST time series. Our improved version of BEAST was the best of all the four detecting changes in LST time series. Moreover, the optimal seasonal harmonic order in the improved BEAST was determined. Our findings are potentially useful for determining the long-term trend dynamic, seasonal variation, and different types of abrupt change detection in LST, which are required for climate change, vegetation monitoring, and environmental studies. Future studies will apply the improved BEAST in LST time series to reveal recent temperature trends.

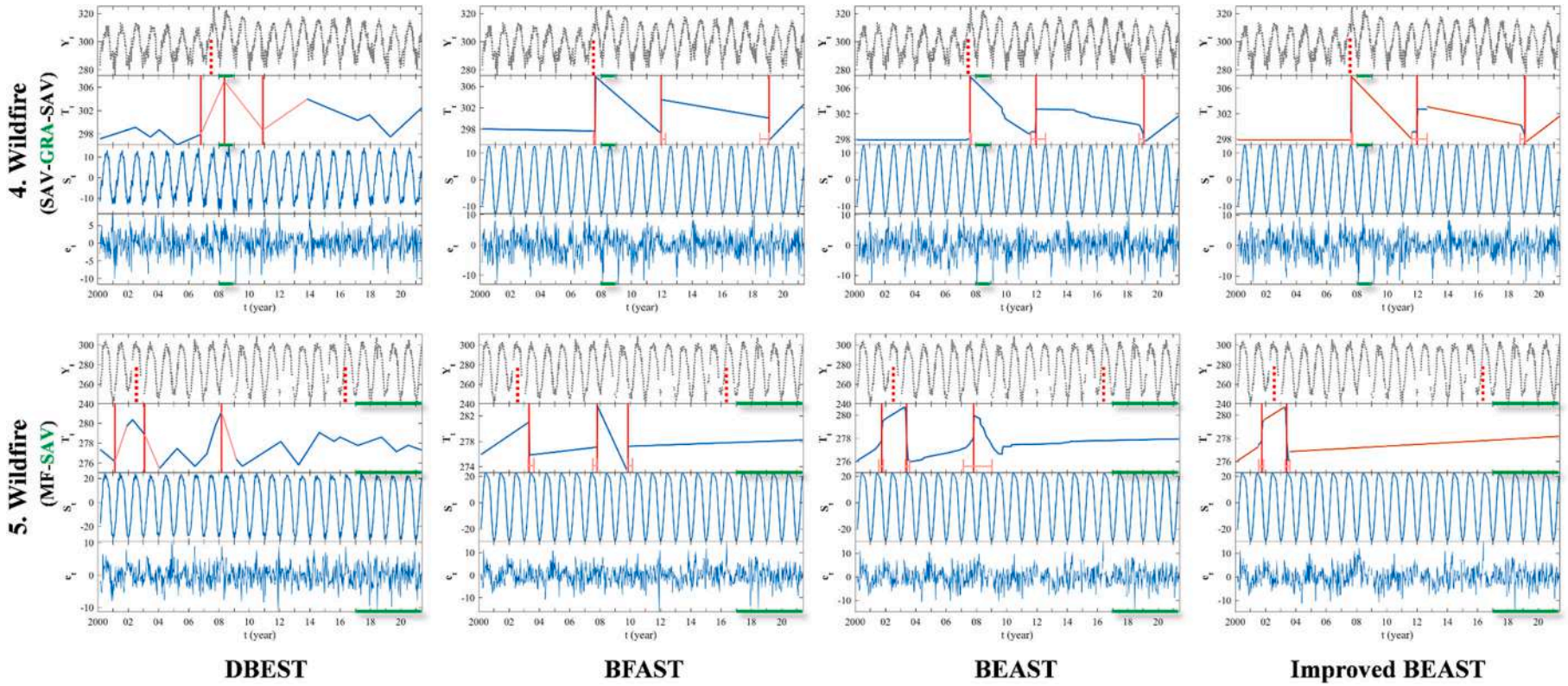

Fig. 17. Same as Fig. 15, but for wildfire detection. Wildfires are displayed as red vertical dotted lines. (For interpretation of the references to colour in this figure legend, the reader is referred to the web version of this article.)

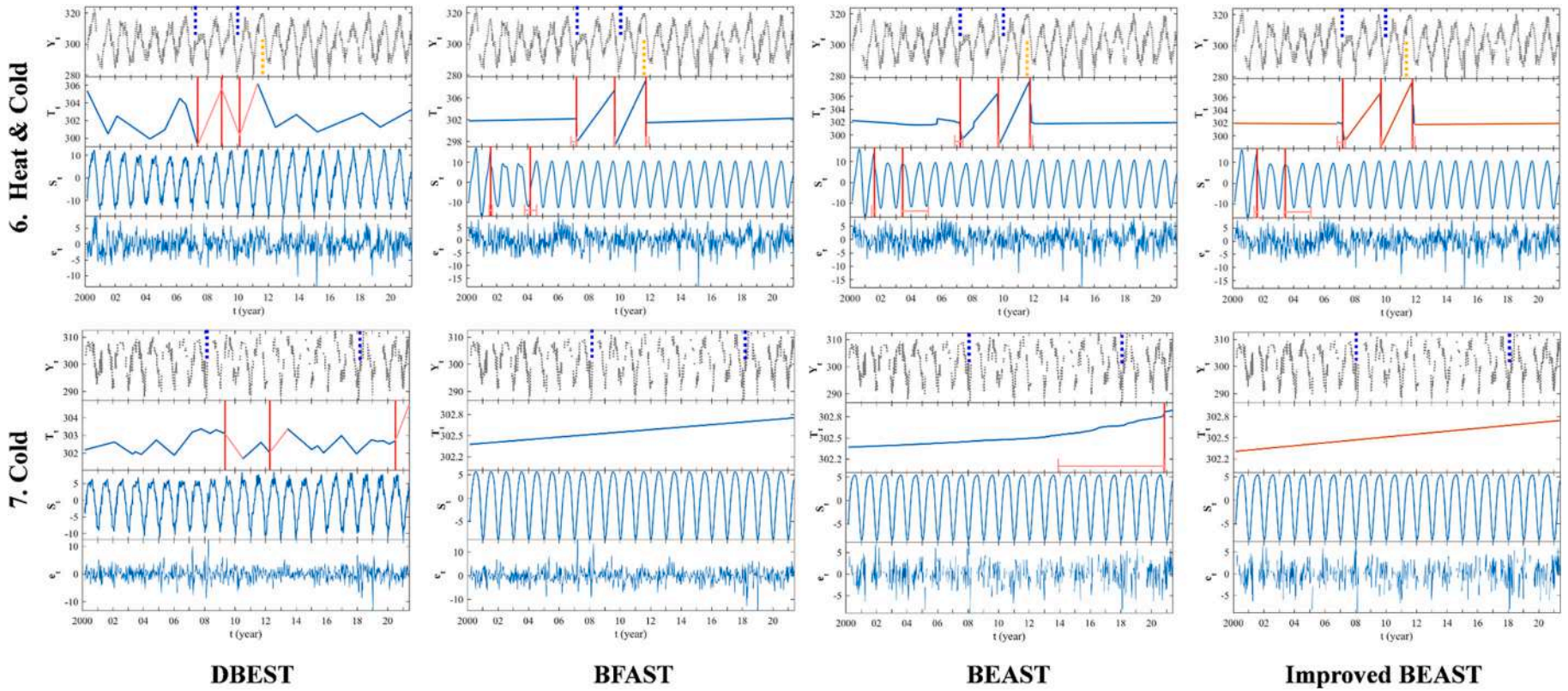

Fig. 18. Same as Fig. 15, but for the heatwave and cold spell detection. Heatwaves are displayed as orange vertical dotted lines and cold spells are represented by blue vertical dotted lines. (For interpretation of the references to colour in this figure legend, the reader is referred to the web version of this article.)

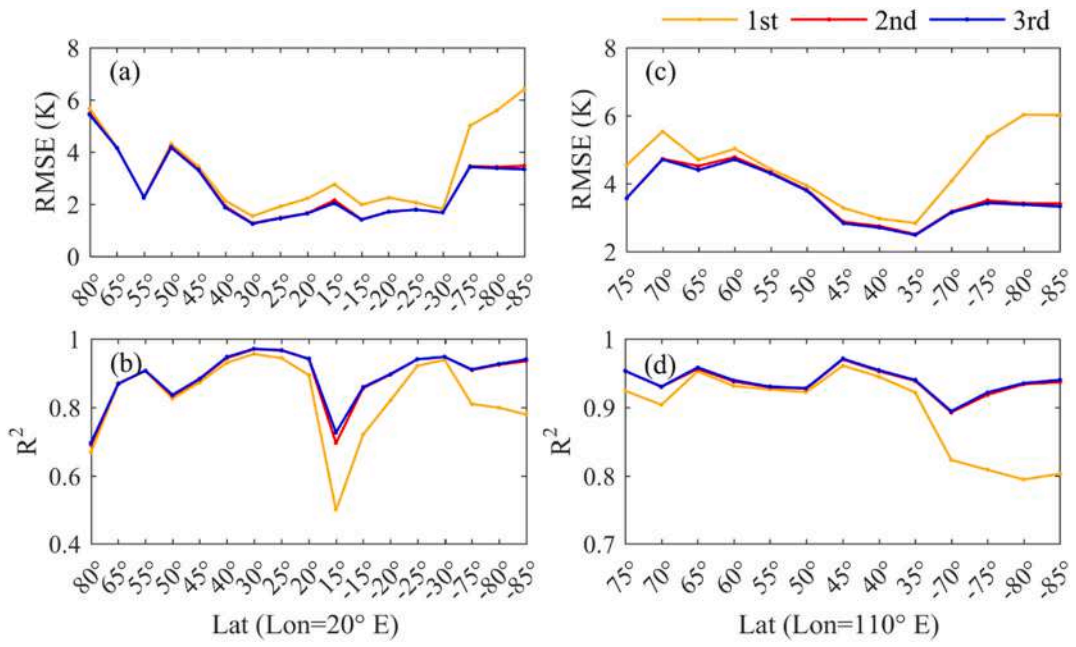

Fig. 19. Changes in RMSE and R^2 of fitted seasonal dynamics using first-order (1st), second-order (2nd), and third-order (3rd) harmonic functions at 20°E and 110°E.

Credit author statement

Jing Li: Investigation, Methodology, Data curation, Formal analysis, Validation, Writing - Original draft.

Zhao-Liang Li: Conceptualization, Methodology, Formal analysis, Supervision, Writing - review & editing.

Hua Wu: Resource, Validation, Writing - review & editing.

Nanshan You: Data curation, Visualization, Writing - review & editing.

Declaration of Competing Interest

No conflict of interest exists.

Acknowledgement

This work was supported by the National Natural Science Foundation of China (Grant No. 41921001, 41871267, and 42071331); and the China Scholar Council (CSC). We thank three anonymous reviewers for their insightful comments.

Appendix A. Supplementary data

Supplementary data to this article can be found online at https://doi.org/10.1016/j.rse.2022.113222.

References

Awty-Carroll, K., Bunting, P., Hardy, A., Bell, G., 2019. An evaluation and comparison of four dense time-series change detection methods using simulated data. Remote Sens. 11, 2779.

Bai, J., Perron, P., 2003. Computation and analysis of multiple structural change models. J. Appl. Econ. 18, 1–22.

Bechtel, B., 2015. A new global climatology of annual land surface temperature. Remote Sens. 7, 2850–2870.

Brooks, E.B., Thomas, V.A., Wynne, R.H., Coulston, J.W., 2012. Fitting the multitemporal curve: a Fourier series approach to the missing data problem in remote sensing analysis. IEEE Trans. Geosci. Remote Sens. 50, 3340–3353.

Brooks, E.B., Wynne, R.H., Thomas, V.A., Blinn, C.E., Coulston, J.W., 2013. On-the-fly massively multitemporal change detection using statistical quality control charts and Landsat data. IEEE Trans. Geosci. Remote Sens. 52, 3316–3332.

Browning, D.M., Maynard, J.J., Karl, J.W., Peters, D.C., 2017. Breaks in MODIS time-series portend vegetation change: verification using long-term data in an arid grassland ecosystem. Ecol. Appl. 27, 1677–1693.

Chinchor, N., 1992. MUC-4 evaluation metrics. In: Proc. of the Fourth Message Understanding Conference, pp. 22–29.

Denison, D.G., Holmes, C.C., Mallick, B.K., Smith, A.F., 2002. Bayesian Methods for Nonlinear Classification and Regression. John Wiley & Sons.

Deyle, E.R., Maher, M.C., Hernandez, R.D., Basu, S., Sugihara, G., 2016. Global environmental drivers of influenza. Proc. Natl. Acad. Sci. U. S. A. 113, 13081–13086.

Estel, S., Kuemmerle, T., Alcántara, C., Levers, C., Prishchepov, A., Hostert, P., 2015. Mapping farmland abandonment and recultivation across Europe using MODIS NDVI time-series. Remote Sens. Environ. 163, 312–325.

Fu, P., Weng, Q., 2016. A time-series analysis of urbanization induced land use and land cover change and its impact on land surface temperature with Landsat imagery. Remote Sens. Environ. 175, 205–214.

Fu, P., Weng, Q., 2018. Variability in annual temperature cycle in the urban areas of the United States as revealed by MODIS imagery. ISPRS J. Photogramm. Remote Sens. 146, 65–73.

Ghent, D., Remedios, J., 2013. Developing first time-series of land surface temperature from AATSR with uncertainty estimates. In: EGU General Assembly Conference Abstracts pp. EGU2013-5016.

Hansen, M.C., Potapov, P.V., Moore, R., Hancher, M., Turubanova, S.A., Tyukavina, A., Thau, D., Stehman, S.V., Goetz, S.J., Loveland, T.R., 2013. High-resolution global maps of 21st-century forest cover change. Science. 342, 850–853.

Huang, F., Zhan, W., Voogt, J., Hu, L., Wang, Z., Quan, J., Ju, W., Guo, Z., 2016. Temporal upscaling of surface urban heat island by incorporating an annual temperature cycle model: a tale of two cities. Remote Sens. Environ. 186, 1–12.

Hurrell, J.W., 1995. Decadal trends in the North Atlantic oscillation: regional temperatures and precipitation. Science. 269, 676–679.

Jaiswal, R., Lohani, A., Tiwari, H., 2015. Statistical analysis for change detection and trend assessment in climatological parameters. Environ. Process. 2, 729–749.

Jamali, S., Jönsson, P., Eklundh, L., Ardö, J., Seaquist, J., 2015. Detecting changes in vegetation trends using time-series segmentation. Remote Sens. Environ. 156, 182–195.

Karl, T.R., Knight, R.W., Baker, B., 2000. The record breaking global temperatures of 1997 and 1998: evidence for an increase in the rate of global warming? Geophys. Res. Lett. 27, 719–722.

Kendall, M., 1975. Rank Correlation Methods, 4th edn. Charles griffin, San Francisco, CA, p. 8.

Khorchani, M., Vicente-Serrano, S.M., Azorin-Molina, C., Garcia, M., Martin-Hernandez, N., Peña-Gallardo, M., El Kenawy, A., Domínguez-Castro, F., 2018. Trends in LST over the peninsular Spain as derived from the AVHRR imagery data. Glob. Planet. Chang. 166, 75–93.

Konapala, G., Mishra, A.K., Wada, Y., Mann, M.E., 2020. Climate change will affect global water availability through compounding changes in seasonal precipitation and evaporation. Nat. Commun. 11, 1–10.

Lark, T.J., Spawn, S.A., Bougie, M., Gibbs, H.K., 2020. Cropland expansion in the United States produces marginal yields at high costs to wildlife. Nat. Commun. 11, 1–11.

Li, Z.-L., Tang, B.-H., Wu, H., Ren, H., Yan, G., Wan, Z., Trigo, I.F., Sobrino, J.A., 2013. Satellite-derived land surface temperature: current status and perspectives. Remote Sens. Environ. 131, 14–37.

Lettenmaier, D.P., 1976. Detection of trends in water quality data from records with dependent observations. Water Resour. Res. 12, 1037–1046.

Li, Y., Liu, Y., Bohrer, G., Cai, Y., Wilson, A., Hu, T., Wang, Z., Zhao, K., 2022. Impacts of forest loss on local climate across the conterminous United States: evidence from satellite time-series observations. Sci. Total Environ. 802, 149651.
Liu, J., Kuang, W., Zhang, Z., Xu, X., Qin, Y., Ning, J., Zhou, W., Zhang, S., Li, R., Yan, C., 2014. Spatiotemporal characteristics, patterns, and causes of land-use changes in China since the late 1980s. J. Geogr. Sci. 24, 195–210.
Lucht, W., Schaphoff, S., Erbrecht, T., Heyder, U., Cramer, W., 2006. Terrestrial vegetation redistribution and carbon balance under climate change. Carbon Balance Manag. 1, 1–7.
Mann, H.B., 1945. Nonparametric tests against trend. Econometrica. 245–259.
Mann, H.B., Whitney, D.R., 1947. On a test of whether one of two random variables is stochastically larger than the other. Ann. Math. Statist. 18, 50–60.
Mudelsee, M., 2019. Trend analysis of climate time-series: a review of methods. Earth-Sci. Rev. 190, 310–322.
Muro, J., Strauch, A., Heinemann, S., Steinbach, S., Thonfeld, F., Waske, B., Diekkrüger, B., 2018. Land surface temperature trends as indicator of land use changes in wetlands. Int. J. Appl. Earth Obs. Geoinf. 70, 62–71.
Patel, N., Kaushal, B.K., 2010. Improvement of user's accuracy through classification of principal component images and stacked temporal images. Geo-spatial Inform. Sci. 13, 243–248.
Pettitt, A.N., 1979. A non-parametric approach to the change point problem. J. Appl. Stat. 28, 126–135.
Potter, C., Tan, P.N., Steinbach, M., Klooster, S., Kumar, V., Myneni, R., Genovese, V., 2003. Major disturbance events in terrestrial ecosystems detected using global satellite data sets. Glob. Chang. Biol. 9, 1005–1021.
Quan, J., Zhan, W., Chen, Y., Wang, M., Wang, J., 2016. Time-series decomposition of remotely sensed land surface temperature and investigation of trends and seasonal variations in surface urban heat islands. J. Geophys. Res. Atmos. 121, 2638–2657.
Robert, C., William, C., Irma, T., 1990. STL: a seasonal-trend decomposition procedure based on loess. J. Off. Stat. 6, 3–73.
Romaguera, M., Vaughan, R.G., Ettema, J., Izquierdo-Verdiguier, E., Hecker, C., Van der Meer, F., 2018. Detecting geothermal anomalies and evaluating LST geothermal component by combining thermal remote sensing time-series and land surface model data. Remote Sens. Environ. 204, 534–552.
Sadmani, M., Safar, M., Roknian, M., 2012. Trend analysis in reference evaporation using Mann Kendall and Spearman' rho test in arid regions of Iran. Water Resour. Manag. 26, 211–224.
Saxena, R., Watson, L.T., Wynne, R.H., Brooks, E.B., Thomas, V.A., Zhiqiang, Y., Kennedy, R.E., 2018. Towards a polyalgorithm for land use change detection. ISPRS J. Photogramm. Remote Sens. 144, 217–234.
Schaefer, D., Domroes, M., 2009. Recent climate change in Japan–spatial and temporal characteristics of trends of temperature. Clim. Past 5, 13–19.
Schwarz, G., 1978. Estimating the dimension of a model. Ann. Stat. 461–464.
Sen, P.K., 1968. Estimates of the regression coefficient based on Kendall's tau. J. Am. Stat. Assoc. 63, 1379–1389.
Song, X.-P., Hansen, M.C., Stehman, S.V., Potapov, P.V., Tyukavina, A., Vermote, E.F., Townshend, J.R., 2018. Global land change from 1982 to 2016. Nature. 560, 639–643.
Stine, A.R., Huybers, P., Fung, I.Y., 2009. Changes in the phase of the annual cycle of surface temperature. Nature. 457, 435–440.
Stocker, T., 2014. Climate Change 2013: The Physical Science Basis: Working Group I Contribution to the Fifth Assessment Report of the Intergovernmental Panel on Climate Change. Cambridge university press.
Tabari, H., Talaee, P.H., Nadoushani, S.M., Willems, P., Marchetto, A., 2014. A survey of temperature and precipitation based aridity indices in Iran. Quat. Int. 345, 158–166.
Theil, H., 1992. A rank-invariant method of linear and polynomial regression analysis. In: Raj, B., Koerts, J. (Eds.), Henri Theil's Contributions to Economics and Econometrics. Springer, pp. 345–381.
Thomson, D.J., 1995. The seasons, global temperature, and precession. Science. 268, 59–68.
Tuomenvirta, H., Alexandersson, H., Drebs, A., Frich, P., Nordli, P.O., 2000. Trends in Nordic and Arctic temperature extremes and ranges. J. Clim. 13, 977–990.
Verbesselt, J., Hyndman, R., Zeileis, A., Culvenor, D., 2010a. Phenological change detection while accounting for abrupt and gradual trends in satellite image time-series. Remote Sens. Environ. 114, 2970–2980.
Verbesselt, J., Hyndman, R., Newnham, G., Culvenor, D., 2010b. Detecting trend and seasonal changes in satellite image time-series. Remote Sens. Environ. 114, 106–115.
Verbesselt, J., Zeileis, A., Herold, M., 2012. Near real-time disturbance detection using satellite image time-series. Remote Sens. Environ. 123, 98–108.
Wang, E., Wang, X., Chen, Y., 2017. The breakpoints detection method using time series of vegetation fractional coverage. J. Geo-inform. Sci. 19 (10), 1355–1363.
Watts, L.M., Laffan, S.W., 2014. Effectiveness of the BFAST algorithm for detecting vegetation response patterns in a semi-arid region. Remote Sens. Environ. 154, 234–245.
Weng, Q., Fu, P., 2014. Modeling annual parameters of clear-sky land surface temperature variations and evaluating the impact of cloud cover using time-series of Landsat TIR data. Remote Sens. Environ. 140, 267–278.
Weng, Q., Lu, D., Schubring, J., 2004. Estimation of land surface temperature–vegetation abundance relationship for urban heat island studies. Remote Sens. Environ. 89, 467–483.
Xing, Z., 2020. Estimation of Daily Mean Land Surface Temperature from Remote Sensing Data and Its Interannual Variation. Chinese Academy of Agricultural Sciences, Beijing.
Xing, Z., Yu, Y., Duan, S.-B., Li, Z.-L., Gao, M., Leng, P., Zhang, X., Shang, G., 2020. Modeling year-to-year variations of clear-sky land surface temperature using aqua/MODIS data. IEEE Access 8, 114541–114553.
Zhang, G., Xiao, X., Dong, J., Kou, W., Jin, C., Qin, Y., Zhou, Y., Wang, J., Menarguez, M. A., Biradar, C., 2015. Mapping paddy rice planting areas through time-series analysis of MODIS land surface temperature and vegetation index data. ISPRS J. Photogramm. Remote Sens. 106, 157–171.
Zhang, Y.-F., Thorburn, P.J., Xiang, W., Fitch, P., 2019. SSIM—A deep learning approach for recovering missing time-series sensor data. IEEE Internet Things J. 6, 6618–6628.
Zhao, K., Wulder, M.A., Hu, T., Bright, R., Wu, Q., Qin, H., Li, Y., Toman, E., Mallick, B., Zhang, X., 2019. Detecting change-point, trend, and seasonality in satellite time-series data to track abrupt changes and nonlinear dynamics: a Bayesian ensemble algorithm. Remote Sens. Environ. 232, 111181.
Zhao, W., Xiong, D., Wen, F., Wang, X., 2020. Lake area monitoring based on land surface temperature in the Tibetan plateau from 2000 to 2018. Environ. Res. Lett. 15, 084033.
Zhu, Z., 2017. Change detection using landsat time-series: a review of frequencies, preprocessing, algorithms, and applications. ISPRS J. Photogramm. Remote Sens. 130, 370–384.
Zhu, Z., Woodcock, C.E., 2014. Continuous change detection and classification of land cover using all available Landsat data. Remote Sens. Environ. 144, 152–171.
Zhu, Z., Zhang, J., Yang, Z., Aljaddani, A.H., Cohen, W.B., Qiu, S., Zhou, C., 2020. Continuous monitoring of land disturbance based on Landsat time-series. Remote Sens. Environ. 238, 111116.